united nations
educational, scientific
and cultural
organization

international atomic
energy agency

the
abdus salam
international centre for theoretical physics

H4.SMR/1241-11

"Workshop on Three-Dimensional Modelling
of Seismic Waves Generation and their Propagation"

25 September - 6 October 2000

UPPER MANTLE ANISOTROPY TOMOGRAPHY

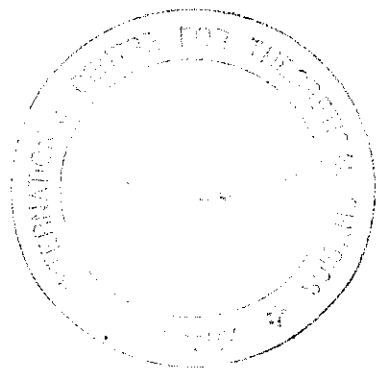

Jean-Paul MONTAGNER

Institut Universitaire de France
Département de Sismologie CNRS UMR 7580
Institut de Physique du Globe
Paris, France

Abstract

The main breakthrough in Seismology during the last ten years, is related to the emergence and development of more and more sophisticated imaging techniques, usually named seismic tomography, at different scales from the local scale up to global scale of the Earth. These progresses have been made it possible by the rapid developments in seismic instrumentation, in electronics, and by the extensive use of massive computation facilities. However, most global tomographic models are suffering severe limitations due to the imperfect data coverage and theoretical approximations. It is usually assumed that the propagating elastic medium is isotropic, which is shown to be a poor approximation. We show in this paper how to take account of anisotropy of Earth's materials. Its influence on the phase of 3 component seismograms is explored. The consequence is that, by including other geological constraints, we are able to map not only the temperature heterogeneities but also the flow field within the convecting mantle. The complete tomographic technique which includes the resolution of a forward problem and of an inverse problem, is described. It is important to emphasize the fact that in order to check the reliability of a tomographic model, it is necessary to calculate the errors and the resolution associated with the model, by considering the structure of the data space (errors and correlations), the parameter space (*a posteriori* errors, covariance function, resolution). However, despite the increasing quality of seismograms provided by modern digital networks (GEOSCOPE, IRIS, ...), the lateral resolution of global is limited to about 1000km and the intallation of ocean bottom observatories constitutes a new challenge for the next century. The recent theoretical developments can be now applied to data in order to use the complete information provided by seismic waveform and to get new insight into anisotropic and anelastic parameters within the Earth, but other solid materials.

1 Introduction

Two kinds of waves, P- and S-waves can propagate inside an elastic medium. For several decades, the main thrust of seismologists was to retrieve reference spherically symmetric Earth models. However, due to the improvement of instruments and measurement techniques, some lateral heteogeneities were evidenced (*Knopoff*, 1972). More than ten years ago, the first global three-dimensionnal tomographic models of P- and S-waves, were published (*Woodhouse and Dziewonski*, 1984; *Dziewonski*, 1984; *Nakanishi and Anderson*, 1984; *Nataf et al.*, 1984, 1986). Since that time, many new tomographic models were published, and a large family of techniques was made available. This important progress was made possible by the extensive use of computers which can handle very large datasets and by the availability of good quality digital seismograms recorded by seismic networks such as the International Deployment of accelerometers (*Agnew et al.*, 1976), the Global Digital Seismograph Network (*Peterson et al.*, 1977) and more recently GEOSCOPE (*Romanowicz et al.*, 1984) and IRIS (*Smith*, 1986). However, most of tomographic techniques only make use of the phase information in seismograms and very few of the amplitude, even when one works on seismic waveform (*Woodhouse and Dziewonski*, 1984). It can be shown (see for example *Montagner*, 1996), from a theoretical and practical point of view, that it is much easier to explain the phase of seismic signals than their amplitude. Therefore, global tomographic models have been improved over years by an increase in the number of data and by more general parameterizations, now including anisotropy (Radial anisotropy in *Nataf et al.* (1986); general slight anisotropy in *Montagner* (1986a) *Montagner and Tanimoto*

(1990, 1991) and to a less extent anelasticity (*Tanimoto*, 1989; *Roult et al.*, *icz*, 1991). However, there is still a major step to perform, in taking a comp amplitude anomalies in the most general case. There were some attempts to do scale (*Tanimoto*, 1984b; *Wong*, 1989) and on a regional scale, following the works er (1988a,b). But, from a practical point of view, it induces inverse problems of very l ge size and it makes it necessary to limit the parameter space to its isotropic part. We show how to take account of seismic anisotropy. Contrarily to the common belief, the anisotropy is not a second order effect and its neglecting can induce some bias on seismic velocities V_P and V_S. The practical implementation of the inverse problem is presented as well as how we can take account of errors on data and how to calculate the resolution and *a posteriori* covariance functions of parameters. Finally, some geodynamic applications will be shown.

2 Anatomy of seismograms

2.1 Progress in instrumentation

Seismology is an observational field which is based on the exploitation of recordings of the displacement (or acceleration) of the Earth induced by earthquakes. It is a very old field since the first Chinese seismoscope dates back one century before Christ. But much progress on seismic instrumentation was done during the last century, though the principle of a seismometer did not change dramatically. It is based on the relative movement of a mass coupled to the Earth motion through a spring or a pendulum (Figure 1). Such a system is characterized by a natural oscillation frequency. However, due to the existence of permanent seismic noise particularly large between 1s. and 10s., there were, for a long time, two different fields in seismology: the short period seismology devoted to periods smaller than 1s and long period seismology for periods longer than 10s.

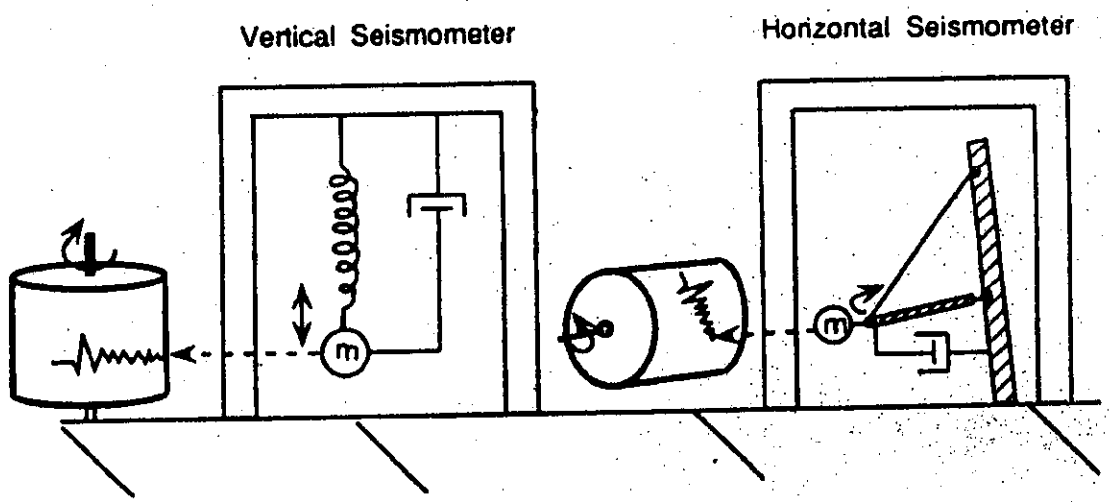

Figure 1: The basic principle of a vertical seismometer with its mass, its spring and damping system

With the development of electronics and force-feedback systems, this gap was filled in the eighties and it is now possible to record the 3 components of seismic displacement, to increase the dynamic range of seismometers as well as their frequency range from 0.1s. up to 1000s. A negative feedback loop enables to apply a force proportional to the inertial mass displacement in order to cancel its relative motion. This approach extends the bandwidth and the linearity of the seismometer. Since the development of STS1 of *Streckeisen and Wielandt* (1982), a new generation of seismometers applying this simple principle, came up. They share common characteristics: they are now light (less than 1 kilogram), have a low power consumption and are very sensitive, robust and reliable. They can detect seismic displacement much smaller than the interatomic distance (10^{-10}m) in the seismic frequency band. An example of such a recent seismometer is presented in figure 2 *(Cacho*, 1996). It is designed to operate in very hostile environments such as planet Mars and seafloor, and it is planned to be used for planetary exploration (*Lognonné et al.*, 1998) and for future ocean bottom stations (*Montagner et al.*, 1998).

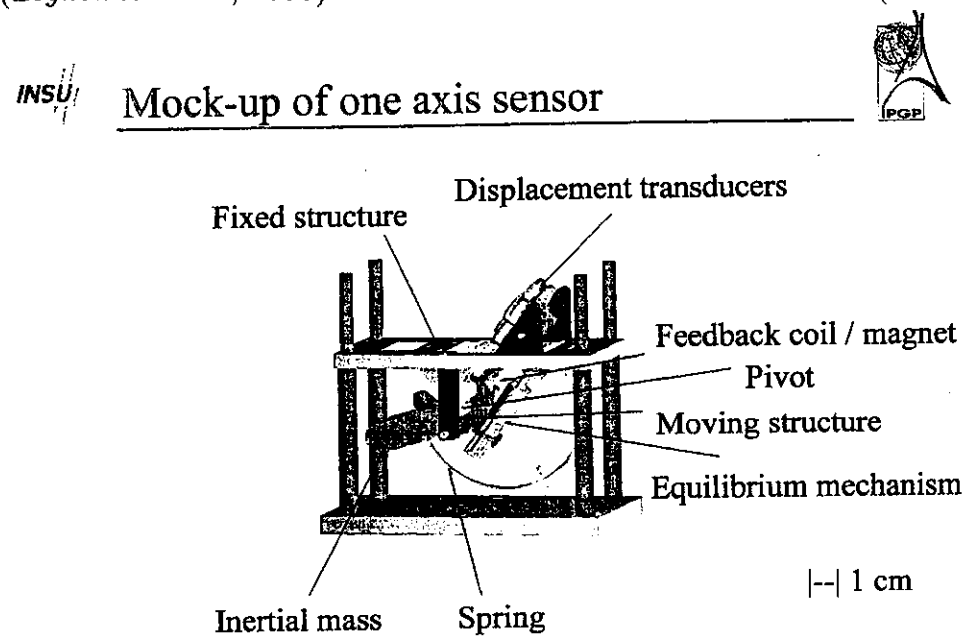

Figure 2: A modern broadband seismometer with its feedback system (*Cacho*, 1996)

The quality of seismograms is no longer related to intrinsic qualities of seismometers but primarily largely dependent on the noise level of the station. A correct station must display a noise level between the low noise model and the high noise model of *Peterson* (1994). The seismic noise is minimum in the period range 20-100s, and at very short periods below 1s. These 2 ranges are separated by the microseismic peak which is due to the complex interaction between fluid Earth (ocean and atmosphere) and solid Earth. The existence of this peak explains why there were traditionnally 2 fields in seismology. It is only since the development of broadband seismometers with a high dynamic range (> 128dB), that both fields have been merged into one field, the broadband seismology.

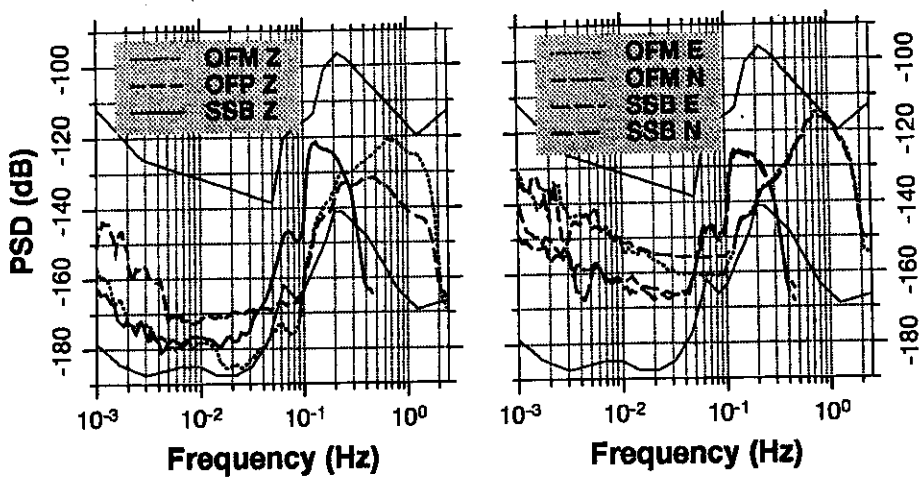

Figure 3: Broadband seismic noise between 0.1s and 1,000s, recorded in SSB (Continental GEOSCOPE station) and on the sea floor during the Sismobs-OFM experiment in may 1992 (*Montagner et al.*, 1994).
The 2 continuous lines correspond to the low-noise and the high-noise models (*Peterson, 1994).*

Broadband 3-component high dynamic seismometers have been installed in more than 200 stations around the world. Their deployment, the definition of a standard format (SEED) and the free availability of data are coordinated through the FDSN (Federation of Digital Seismograph Networks, Figure 4). It is worthwile to notice that the whole community of seismologists accepted to share their data. However, despite these international efforts, there are still many areas at the surface of Earth devoided of broadband seismic stations. These regions are primarily located in southern hemisphere and more particularly in oceanic areas where no island is present. Therefore, an international effort is ongoing, coordinated through I.O.N. (International Ocean Network) in order to promote the installation of geophysical ocean bottom observatories in order to fill the enormous gaps in the station coverage (*Suyehiro et al.*, 1995).

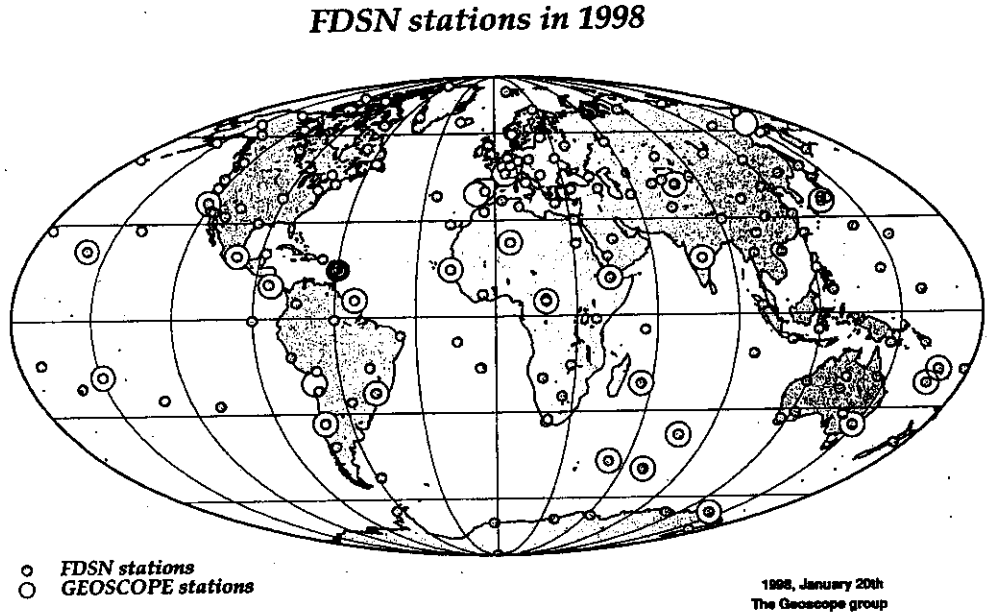

Figure 4: Distribution of the broadband standardized stations of FDSN network

2.2 Body waves, surface waves and normal modes

A seismic record is characterized by its natural complexity, looking like a "chaotic" series of wiggles, well above seismic noise. The basic job of a seismologist will consist in unraveling the succession of impulsive arrivals, and to distinguish the body waves from the following complex dispersed wavetrains, the surface waves. Figure 5 shows an example of 3-component broadband seismograms for an earthquake located in Chile, of magnitude 7.3 recorded in the GEOSCOPE station of Canberra in Australia. The horizontal component seismograms (North-South and East-West) have been rotated into longitudinal and transverse components, in order to separate different kinds of body waves and surface waves. The seismic noise can be quantitatively assessed by considering the level of unexplained signal before the first arrival of P-waves. Most of the largest impulses can be explained by reflected or refracted waves at the major seismic discontinuities, i.e. the surface of the Earth (PP, SS, SSS, PS), the core-mantle boundary (Pdiff, SKS, ...) at 2900km depth and the ICB (inner core boundary). The nomenclature of all these body waves is explained in figure 6, and is reflecting the propagation history of waves in the 3 main layers of the Earth, i.e. the mantle, the outer core and the inner core.

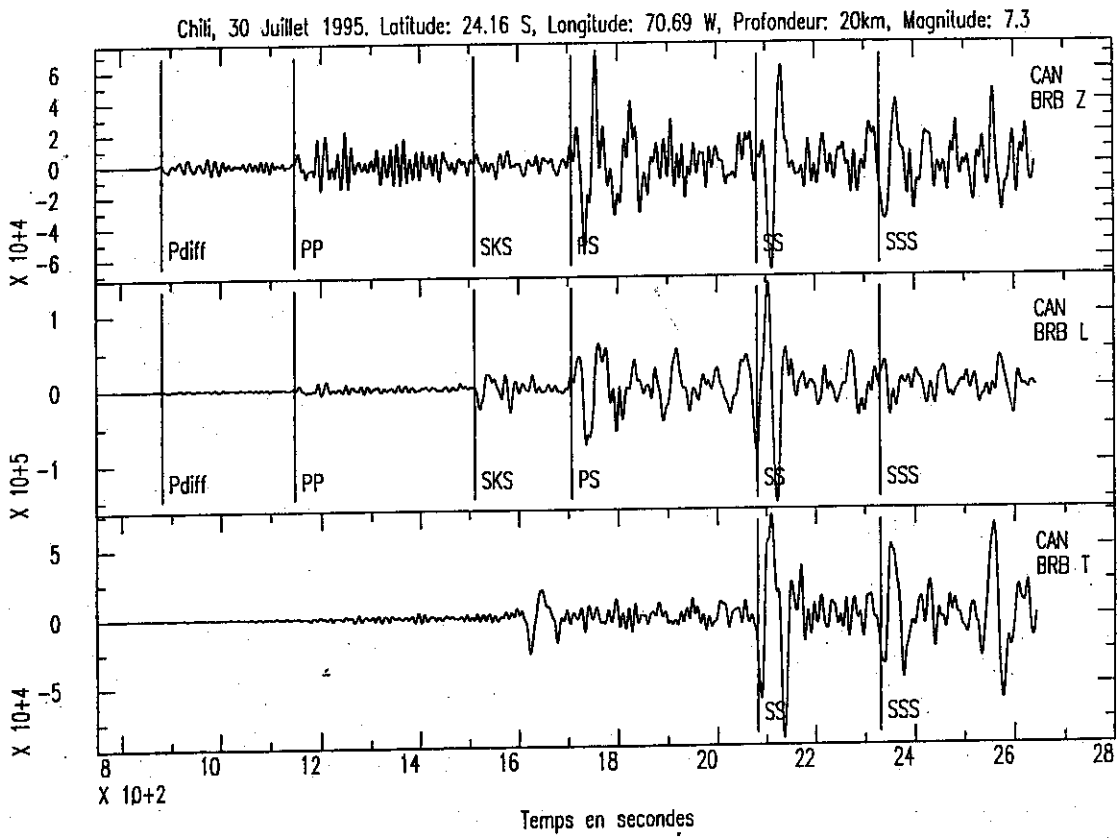

Figure 5: Example of 3-component broadband seismogram recorded in the GEOSCOPE station CAN, for a Chilean Earthquake of magnitude 7.3

Figure 6: Seismic rays through the Earth: explanation of the nomenclature

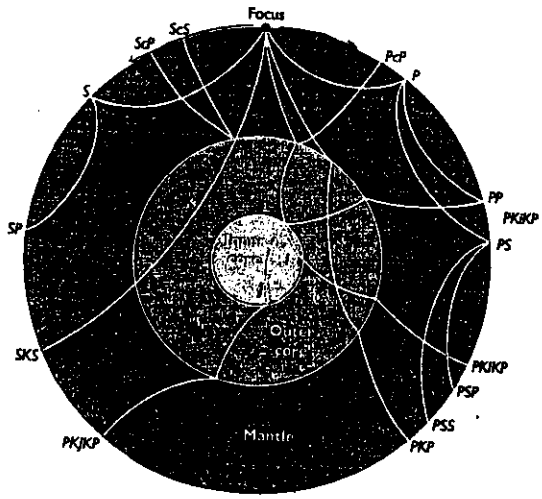

Surface waves are arriving after body waves, and are the most energetic waves at large distances and at long periods. Figure 7 shows seismograms for the same earthquake as in figure 5, but for a longer and low pass filtered time series (T>100s). Two kinds of surface waves are observed: Love waves on the transverse component corresponding to SH- guided waves, and Rayleigh waves on the vertical and longitudinal components resulting from the complex coupling of P- and SV- waves. Their group velocities are approximately 4.3km/s for Love waves and 4km/s for Rayleigh waves.

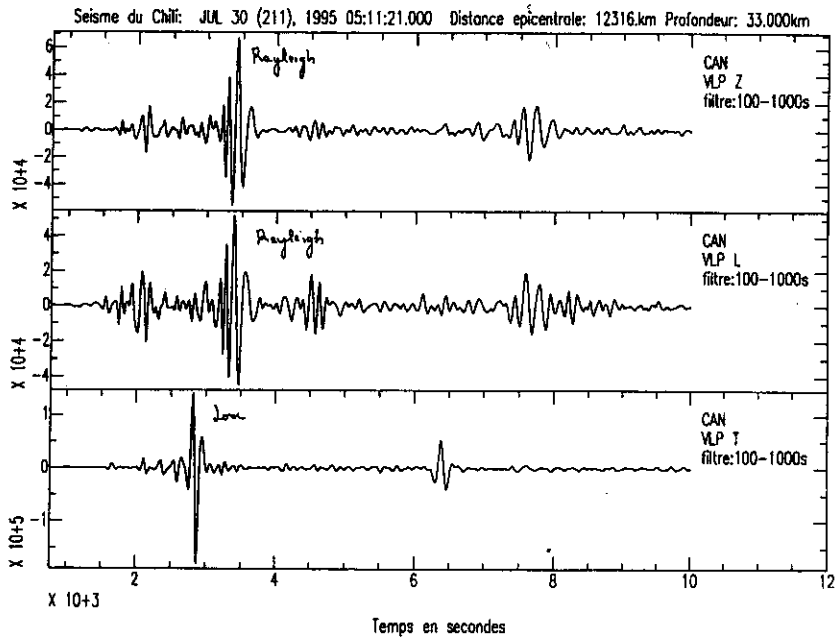

Figure 7: Low pass-filtered (T>100s) seismogram recorded in the GEOSCOPE station CAN for the same earthquake as in figure 5.

When considering even longer time series (more than one day) following very large earthquakes (magnitude larger than 7), it is possible to display the free oscillations of the Earth. Figure 8a shows an example of 2 days of record at the Santa Cruz station (California) of the large Kurile earthquake which occurred in october 94. The spectrum calculated for the first 3 hours of record on 3 components (Figure 8b) does not present any specific characteristics. It is primarily reflecting the convolution of the source time function with the transfer function of the Earth between the epicenter and the station. But, if we calculate the spectrum on a 36 hours time series (Figure 8c), very narrow peaks are come up. They can be explained by the constructive interference between stationary waves traveling in opposite directions. These well defined frequencies are named eigenfrequencies, and are characteristics of the structure of the Earth as well as sounds are characteristics of a string of guitar. They constitute the base of the Earth spectroscopy. The modes on the transverse component (toroidal modes related to Love waves and SH waves) are different from the ones visible on the vertical and longitudial component (Spheroidal modes related to Rayleigh waves resulting from the coupling between P and SV waves). We will briefly review how the eigenfrequencies and the corresponding eigenfunctions can be calculated in a spherically symmetric reference Earth model.

Figure 8: Spectra of the seismograms corresponding to 2 different time series, of the Kuriles Earthquake, Oct. 94, recorded at the station Santa Cruz in California. 8a: 2 days time series. 8b: spectrum for the first 3 hours of the record. 8c: spectrum for the first 36 hours

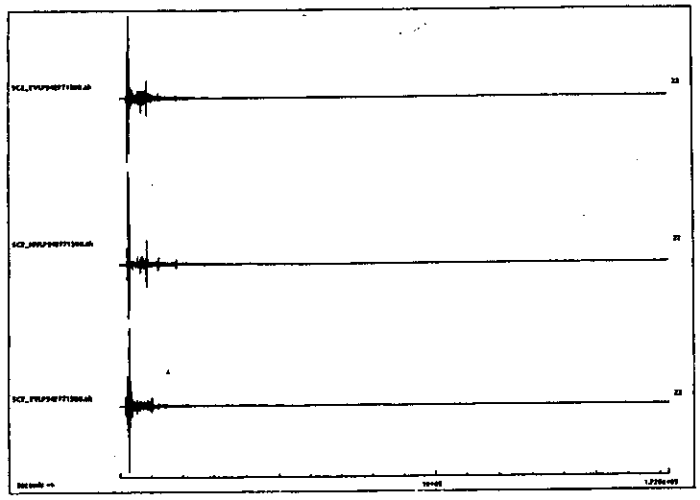

KURIL 94 277 - SCZ VLP - 3h.

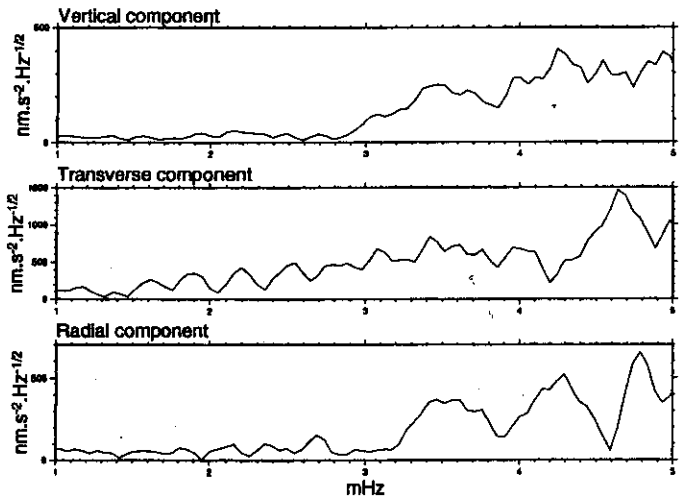

KURIL 94 277 - SCZ VLP - 36h.

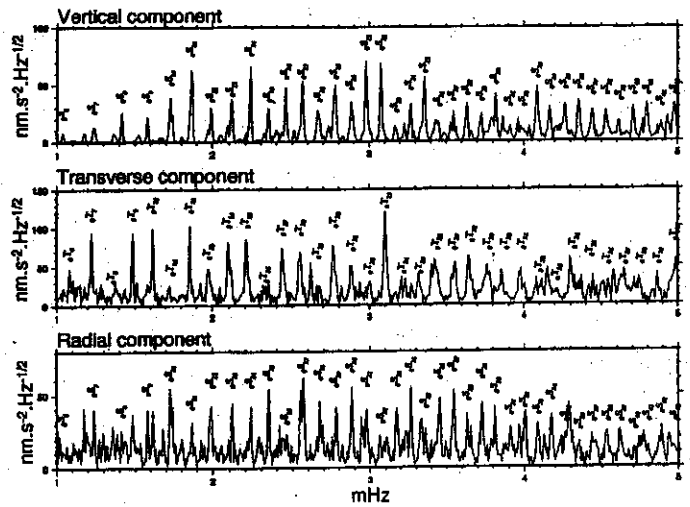

2.3 Normal Mode Theory

The basic equation which governs the displacement $\mathbf{u}(\mathbf{r},t)$ is the elasto-dynamics equation:

$$\rho_0 \frac{d^2 u_i}{dt^2} = \sum_j \sigma_{ij,j} + f_{Si} + f_{Ei} \tag{1}$$

f_{Si} et f_{Ei} represent respectively the whole ensemble of applied inertial and external forces (see *Woodhouse and Dahlen* , (1978) for a complete description of all terms). Generally, by neglecting the advection term, this equation is written in a simple way:

$$(\rho_0 \partial_{tt} - H_0)\mathbf{u}(\mathbf{r},t) = \mathbf{f}(\mathbf{r_S},t) \tag{2}$$

where H is an integro-differential operator and $\mathbf{f}$ expresses all forces applied to the sourve point in $\mathbf{r_S}$ at time t. We assume that $\mathbf{f}$ is equal to 0 for $t < 0$. In the elastic case, there is a linear relationship between σ_{ij} and the strain tensor ϵ_{kl}. $\sigma_{ij} = \sum_{kl} \Gamma_{ijkl}\epsilon_{kl}$ (+ terms related to the initial stress). Γ_{ijkl} is a 4^{th}-order tensor. By using the different symmetry conditions $\Gamma_{ijkl} = \Gamma_{jikl} = \Gamma_{ijlk} = \Gamma_{klij}$, the tensor $\mathbf{\Gamma}$ is shown to have 21 independent elastic moduli.
When we are looking for the free oscillations of the Earth, we assume that $\mathbf{f} = 0$. The solution $\mathbf{u}(\mathbf{r},t)$ of the equation (2) can be calculated for a spherically symmetric non rotating reference Earth model M_0, associated with the operator H_0, according to the equation:

$$\rho_0 \partial_{tt}\mathbf{u}(\mathbf{r},t) = H_0\mathbf{u}(\mathbf{r},t) \tag{3}$$

The eigenvalues of the operator H_0 are equal to $-\rho_0 {}_n\omega_\ell^2$ where ${}_n\omega_\ell$ is the eigenfrequency characterized by 2 quantum numbers n and ℓ, respectively termed radial and angular orders. The corresponding eigenfunctions ${}_n\mathbf{u}_\ell^m(\mathbf{r},t)$ are dependent on 3 quantum numbers n, ℓ, m, where m is the azimuthal order, with the following property $-\ell \leq m \leq \ell$. Therefore, for a given eigenfrequency ${}_n\omega_\ell$ calculated in a spherically symmetric Earth model, $2\ell + 1$ eigenfunctions can be defined. The eigenfrequency ${}_n\omega_\ell$ is said to be degenerated, with a degree of degeneracy $2\ell + 1$. There is a complete formal similarity with lhe calculation of the energy levels of the atom of hydrogen in quantum mechanics.
The eigenfunctions ${}_n\mathbf{u}_\ell^m(\mathbf{r},t)$ of the operator H_0 are orthogonal and normalized. The displacement ${}_n\mathbf{u}_\ell^m(\mathbf{r},t)$ associated with the mode n, ℓ, m can be written:

$${}_n\mathbf{u}_\ell^m(\mathbf{r},t) = {}_n\mathbf{D}_\ell\, Y_\ell^m(\theta,\phi)e^{i{}_n\omega_\ell t} \tag{4}$$

where

$${}_n\mathbf{D}_\ell = {}_nU_\ell(r)\mathbf{r} + {}_nV_\ell(r)\nabla_1 + {}_nW_\ell(r)(-\mathbf{r}\times\nabla_1) \tag{5}$$

where ${}_nU_\ell$, ${}_nV_\ell$, and ${}_nW_\ell$ are the radial eigenfunctions of spheroidal and toroidal modes. $Y_\ell^m(\theta,\phi)$ are spherical harmonics normalized according to Edmonds (1960) and ∇_1 is the surface gradient operator on the unit sphere.
The important point is that the basis of functions defined by equation (4) is complete. That involves that any displacement at the surface of the Earth can be expressed as a linear combination of these eigenfuctions:

$$\mathbf{u}(\mathbf{r},t) = \sum_{n,\ell,m} {}_na_l^m\, {}_n\mathbf{u}_\ell^m(\mathbf{r},t)$$

Therefore, these eigenfunctions can be used for calculating the displacement at any point $\mathbf{r}$, at time t, due to a point force system $\mathbf{F}$ at point $\mathbf{r}_S$ and a step time function, which is a good starting model for earthquakes. The solution of the equation, $\rho_0 \partial_{tt}\mathbf{u}(\mathbf{r},t) = H_0\mathbf{u}(\mathbf{r},t) + \mathbf{F}$ is given by:

$$\mathbf{u}(\mathbf{r},t) = \sum_{n,\ell,m} -{}_n\mathbf{u}_\ell^m(\mathbf{r}) \frac{cos_n\omega_\ell t}{{}_n\omega_\ell^2} e^{\frac{-n\omega_\ell t}{2Q}} ({}_n\mathbf{u}_\ell^m . \mathbf{F})_S \tag{6}$$

The source term $({}_n\mathbf{u}_\ell^m . \mathbf{F})_S$ can be replaced, by using Green's theorem by:

$$({}_n\mathbf{u}_\ell^m . \mathbf{F})_S = (\mathbf{M} : \epsilon)_S$$

where $\mathbf{M}$ and ϵ are respectively the seismic moment tensor and the deformation tensor. Both tensors are symmetric. Since the equation (6) is linear in $\mathbf{M}$, it can be easily generalized to more complex spatial and temporal source functions, and can be rewritten:

$$\mathbf{u}(\mathbf{r},t) = \mathbf{G}(\mathbf{r},\mathbf{r_S},t,t_S)\mathbf{M}(\mathbf{r_S},t_S)$$

where $\mathbf{G}(\mathbf{r},\mathbf{r_S},t,t_S)$ is the Green operator of the medium. The normal mode theory is routinely used for calculating synthetic seismograms at long periods ($T \geq 40s.$) and the agreement between synthetic and observed seismograms is quite good, as is shown in figure 9.

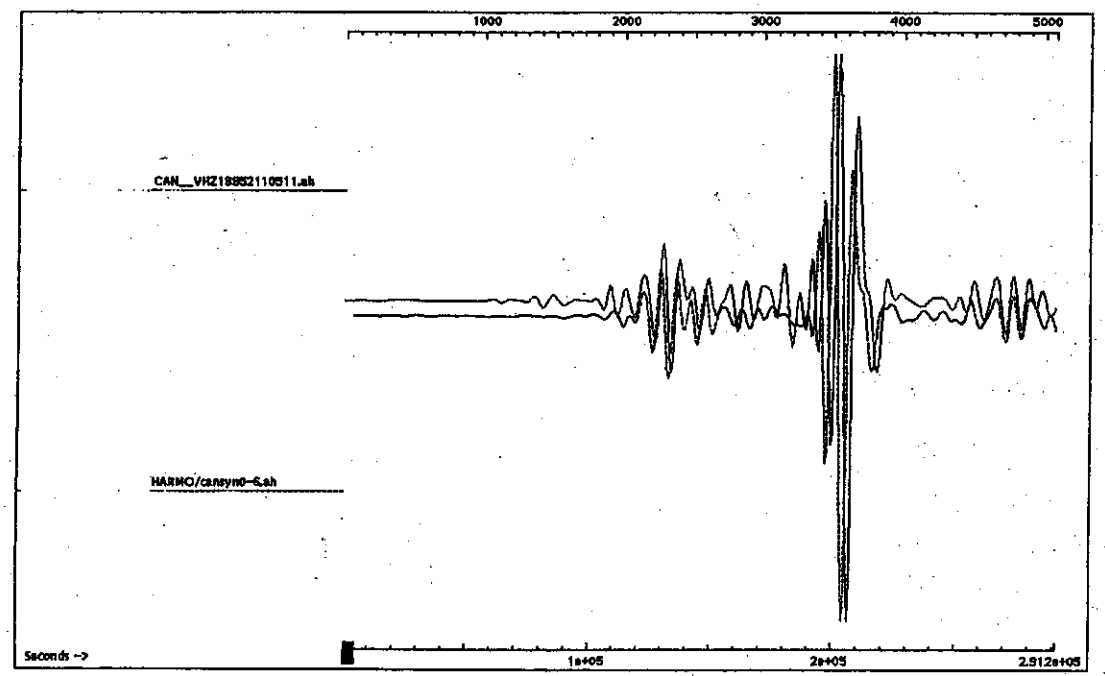

Figure 9: Observed and synthetic seismograms calculated for the Chile earthquake of July 95 in the GEOSCOPE station Canberra.

However, it can be seen that some frequency dependent time shift is still present between the observed and synthetic seismogram. The goal of seismology is to explain this anomaly: that means that some of the hypotheses considered for calculating the synthetic seismograms are insufficient. The simplest way to explain the time delay consists in removing the assumption

that the Earth is spherically symmetric, or in other words that there are lateral heterogeneities between the source and the receiver. The next issue consists in characterizing these lateral heterogeneities. Since the agreement between synthetic and observed seismogram is correct at long periods, we can reasonably infer that the amplitude of heterogeneities is small. Behind the surface wave train, a long coda is usually observed, interpreted as scattered waves. However, when filtering out the periods shorter than 40s., this coda wave vanishes, which means that the scattering effect is only present in the shallowest regions of the Earth (primarily the crust) but that it is probably negligible at largest depths. Therefore, we make the hypothesis that the scale of lateral heterogeneities is large compared with the wavelength. A second hypothesis which has to be discussed, is the isotropic nature of the Earth materials. Actually it is a poor assumption, because seismic anisotropy can be undoubtedly observed at different scales.

3 An anisotropic Earth

3.1 Seismic anisotropy at all scales

Different geophysical fields are involved in the investigation of the manifestations of anisotropy of Earth materials: mineral physics and geology for the study of the microscopic scale, and seismology for scales larger than typically one kilometer. The different observations related to anisotropy, at different scales are reviewed in *Montagner* (1998).

• *Microscopic scale.*

The different minerals present in the upper mantle are strongly anisotropic (*Peselnick et al.*, 1974). The difference of velocity between the fast axis and the slow axis is larger than 20% for olivine the main constituent of the upper mantle. Other important constituents such as orthopyroxene or clinopyroxene are anisotropic as well ($> 10\%$) (see *Anderson*, 1989, *Babuska and Cara*, 1991 for reviews). However, some other constituents such as garnet, display a cubic crystallographic structure which presents a small anisotropy. Consequently, the petrological models which are assemblages of different minerals are less anisotropic than pure olivine. The amount of anisotropy is largely dependent on the percentage of these different minerals and on the mechanisms which align the crystallographic axes according to preferred orientations. For example, the anisotropy of the pyrolitic model, mainly composed of olivine and orthopyroxene (*Ringwood*, 1975), will depend on the relative orientation of the crystallographic axes of different constituents (*Christensen and Lundquist*, 1982). However, through the mechanisms of lattice preferred orientation, its anisotropy can be larger than 10% (*Montagner and Anderson*, 1989a). For competing petrological models such as piclogite (*Anderson and Bass*, 1984, 1986), where the percentage of olivine (respectively garnet) is smaller (resp. larger), the amount of anisotropy is smaller (about 5%). Therefore, at microscopic scales, we can conclude that earth materials in the upper mantle are strongly anisotropic, but that the anisotropy tends to decrease as depth is increasing.

At slightly larger scales, the scale of rock samples, several studies of anisotropy were undertaken. Dunite, which is almost pure olivine, displays a large anisotropy (*Peselnick and Nicolas*, 1978). Moreover, this anisotropy is coherent in whole massifs of ophiolites over several tens of kilometers (*Nicolas*, 1993; *Vauchez and Nicolas*, 1991). Some attempts have been undertaken to numerically model seismic anisotropy within convecting cells (*Ribe*, 1989). At larger wavelengths, anisotropy is also present and can be investigated from seismic observations.

• *Macroscopic scale*:
Different and independent seismic datasets make evident that the effect of anisotropy is not negligible for explaining the propagation of seismic waves inside the Earth. From a seismological point of view, there is no longer doubt that the upper mantle is anisotropic. The early evidence was the discrepancy between Rayleigh and Love wave dispersion (*Anderson*, 1961; *Aki and Kaminuma*, 1963) and the azimuthal dependence of P_n velocities (*Hess*, 1964). Azimuthal variations are now well documented for different areas in the world for body waves and surface waves.
For body waves, this kind of informations results from the investigation of the splitting in teleseismic shear waves such as SKS (*Vinnik et al.*, 1984; 1989a,b; 1991; 1992), ScS [*Ando*, 1984; *Fukao*, 1984) and S (*Ando et al.*, 1983; *Bowman and Ando*, 1987). Since these pioneering papers, many studies have confirmed the existence of splitting of S-waves. These waves are shown to provide an excellent lateral resolution, if we restrict to the deep upper mantle (i.e. below crust). And among these different observations, the splitting information derived from SKS is the less ambiguous and has been extensively used in teleseismic anisotropy investigations (*Silver and Chan*, 1988; *Vinnik et al.*, 1989a,b; *Ansel and Nataf*, 1989; *Silver*, 1996; ...). The drawback of this technique is that it is almost impossible to locate at depth the anisotropic area.
Surface waves are also well suited for investigating the upper mantle anisotropy. Two kinds of observable anisotropy can be considered: The radial anisotropy which results from the discrepancy between Love and Rayleigh waves, also named the "polarization" anisotropy or radial anisotropy. In order to remove this discrepancy, it is necessary to consider a transversely isotropic model with a vertical symmetry axis. This kind of anisotropy is characterized by 5 elastic parameters plus density (*Anderson*, 1961). However, *Levshin and Ratnikova* (1984) showed that lateral heterogeneity can lead to a Rayleigh-Love discrepancy and that we must be cautious about the interpretation of this discrepancy in terms of anisotropic model. On a global scale, *Nataf et al.* (1984; 1986) have derived by the simultaneous inversion of Rayleigh and Love wave dispersion, the geographical distributions of S-wave anisotropy at different depths assuming transverse isotropy with vertical symmetry axis.
The second kind of observable anisotropy is the azimuthal anisotropy which was directly derived from the azimuthal variation of phase velocity. It was observed for the first time on surface waves in Nazca plate by *Forsyth* (1975). Several global and regional models have been derived for both kinds of anisotropy (*Mitchell and Yu*, 1980; *Montagner*, 1985). *Tanimoto and Anderson* (1985) obtained a global distribution of the Rayleigh wave azimuthal anisotropy at long periods. On a regional scale, several tomographic investigations report the existence of azimuthal anisotropy in the Indian Ocean (*Montagner*, 1986a; *Debayle and Lévêque*, 1998), in the Pacific ocean (*Suetsugu and Nakanishi*, 1987; *Nishimura and Forsyth*, 1987, 1988), in the Atlantic ocean (*Silveira et al.*, 1998), in Africa (*Hadiouche et al.*, 1989) and in Central Asia (*Griot et al.*, 1998a,b). *Lévêque and Cara* (1985), *Cara and Lévêque* (1988) used higher mode data to display anisotropy under the Pacific Ocean and North America down to at least 300km.
However, the "polarization" anisotropy (or radial anisotropy) and the azimuthal anisotropy are two different manifestations of a same phenomenon: the anisotropy of the upper mantle. *Montagner and Nataf* (1986) derived a technique which makes it possible to simultaneously explain these two forms of seismically observable anisotropy. The principles of this technique will be described in section 3.2, for the most general case of anisotropy (at the condition that it

is weak). The method can be slightly simplified by introducing only one symmetry axis (7 independent anisotropic parameters) and it was coined "Vectorial tomography" (*Montagner and Nataf*, 1988). It was applied to the investigation of the Indian Ocean (*Montagner and Jobert*, 1988) and of Africa (*Hadiouche et al.*, 1989). These different investigations showed that, paradoxically, *a parameterization with anisotropy requires less parameters than a parameterization with only isotropic terms.* Contrarily to body waves, surface waves enable to locate at depth anisotropy but, so far, its lateral resolution (several thousands kilometers) is very poor.
Finally, anisotropy has not only an effect on the phase of seismograms, but also on its amplitude. Due to the coupling between surface wave modes, one of the less ambiguous effect is the fact that Love waves can be present on the vertical and the radial components (*Park and Yu*, 1993). It can be also displayed from the observations of polarization anomalies too large to be explaind by deviations due to isotropic heterogeneities (*Laske and Masters* , 1998; *Larson et al.*, 1998). Therefore, seismic anisotropy cannot be considered as a second order effect. It is present at different scales and at different depths. We note that it tends to decrease as wavelength is increasing, from 20% at microscopic scale down to $1-2\%$ at very large wavelengths. Several conditions must be fulfilled in order to observe anisotropy at long period and large wavelength. The material must be microscopically anisotropic, there must be some efficient mechanism of preferred orientation, which aligns fast axis (or slow axis) of minerals in the flow field. There must be in addition an efficient strain field, with a long wavelength coherency, for spatial wavelengths Λ_S such that $\Lambda_S \gg \lambda$ (where λ is the wavelength of the wave). This kind of condition is usually encountered in many areas all around the world. Body wave anisotropy and surface wave anisotropy can be related in the simple case of anisotropy characterized by a horizontal symmetry axis (*Montagner et al.*, 1999).
We will now explain how to simultaneously explain the different observations of surface wave anisotropy, radial anisotropy and azimuthal anisotropy.

3.2 First order perturbation theory in the plane case

We will only consider the propagation of surface waves in the plane case, but it can be easily extended to the spherical Earth (*Montagner*, 1996). In the simple plane case (fundamental modes, no coupling between branches of Rayleigh and Love waves), the frequency shift, for a constant wavenumber k can be written:

$$\delta\omega|_k = -\frac{1}{2\omega}\frac{\langle \mathbf{u}_k|\mathbf{E}^{\mathbf{T}}\,\mathbf{\Gamma}\,\mathbf{E}|\mathbf{u_k}\rangle}{\langle \mathbf{u}_k|\rho_0|\mathbf{u_k}\rangle} \tag{7}$$

where E and Γ are respectively the deformation and the elastic tensors, $|\mathbf{u_k}\rangle$ the eigenfunctions as defined in equation (4), where k is corresponding to the multiplet of the 3 quantum numbers (n, ℓ, m). Let us follow the same approach as *Montagner and Nataf* (1986) for calculating $\delta\omega|_k$, where we consider the propagation of the fundamental modes of Love and Rayleigh waves in an arbitrarily stratified half- space in which a right-handed Cartesian coordinate system (x, y, z) is defined on figure 10:

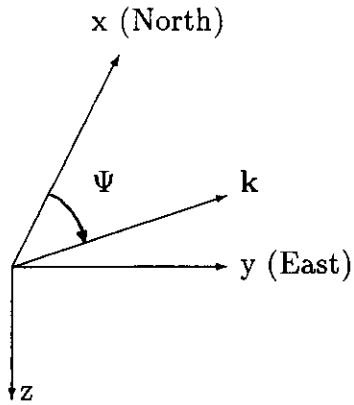

Figure 10: Definition of the Cartesian coordinate system (x, y, z) used in the calculations. Ψ is the azimuth with respect to North of the wavevector.

The half-space is assumed to be homogeneous and may be described by its density $\rho(z)$ and its 4th-order elastic tensor $\Gamma(z)$ with 21 independent elastic coefficients. All these parameters are so far supposed independent of x and y coordinates (z is the vertical component). This condition will be released in the next section. The unperturbed medium is assumed isotropic with an elastic tensor $\Gamma_0(z)$. In that medium, the two cases of Love and Rayleigh wave dispersion can be successively considered.
The unperturbed Love wave displacement is of the form:

$$\mathbf{u}(\mathbf{r},t) = \begin{pmatrix} -W(z)\sin\Psi \\ W(z)\cos\Psi \\ 0 \end{pmatrix} exp(i[k(x\cos\Psi + y\sin\Psi) - \omega t]) \tag{8}$$

where $W(z)$ is the scalar depth eigenfunction for Love waves, k is the horizontal wave number, and Ψ is the azimuth of the wave number k measured clockwise from the North.
The unperturbed Rayleigh wave displacement is of the form:

$$\mathbf{u}(\mathbf{r},t) = \begin{pmatrix} V(z)\cos\Psi \\ V(z)\sin\Psi \\ iU(z) \end{pmatrix} exp(i[k(x\cos\Psi + y\sin\Psi) - \omega t]) \tag{9}$$

where $V(z)$ and $U(z)$ are the scalar depth eigenfunctions for Rayleigh waves. The associated strain tensor $\epsilon(\mathbf{r},\mathbf{t})$ is defined by:

$$\epsilon_{ij}(\mathbf{r},t) = 1/2(u_{i,j} + u_{j,i}) \tag{10}$$

where $,j$ denotes the differentiation with respect to the j-th coordinate. The medium is perturbed from $\Gamma_0(z)$ to $\Gamma_0(z) + \gamma(z)$, where $\gamma(z)$ is small compared to $\Gamma_0(z)$ but quite general in the sense that there is no assumption on the kind of anisotropy. This means that we are in the approximation where we can still consider quasi-Love modes and quasi-Rayleigh modes (*Crampin*, 1984). From Rayleigh's principle, the first order perturbation $\delta C(\mathbf{k})$ in phase velocity dispersion is (*Smith and Dahlen*, 1973, 1975):

$$\delta C(\mathbf{k}) = \frac{C}{2\omega^2} \frac{\int_0^\infty \gamma_{ijkl}\epsilon_{ij}\epsilon_{kl}^*}{\int_0^\infty \rho_0 u_k u_k^* dz} dz \tag{11}$$

where u_i and ϵ_{ij} are respectively the displacement and the strain for the unperturbed half-space and the asterisk denotes complex conjugation.
Now because of the symmetry of the tensors $\gamma(z)$ and ϵ, we use the simplified index notation c_{ij} and ϵ_i for the elements γ_{ijkl} and ϵ_{ij}, but we must take account of the number n_{ij} of coefficients γ_{ijkl} for each c_{ij}. The simplified index notation for the elastic tensor γ_{ijkl} is defined in a coordinate system (x_1, x_2, x_3) by:

$$\gamma_{ijkl} \longrightarrow c_{pq} \begin{cases} \text{if } i = j \Rightarrow & p = i \\ \text{if } k = l \Rightarrow & q = k \\ \text{if } i \neq j \Rightarrow & p = 9 - i - j \\ \text{if } k \neq l \Rightarrow & q = 9 - k - l \end{cases} \tag{12}$$

This kind of transformation enables to relate the 4^{th} order tensor Γ (3x3x3x3) to a matrix c (6x6). The same simplified index notation can be applied to the components of the strain tensor ϵ_{ij}, transforming the 2^{nd} order tensor ϵ (3x3) into a vector with 6 components. However, it is necessary to be careful, because to a given c_{pq} corresponds several γ_{ijkl}, and γ_{ijkl} must be replaced by $n_{pq}c_{pq}$, where n_{pq} is the number of γ_{ijkl} giving the same c_{pq}. Therefore, the equation (25) expressing Rayleigh's principle can be rewritten as:

$$\delta C(\mathbf{k}) = \frac{C}{2\omega^2} \frac{\int_0^\infty \sum_{ij} n_{ij} c_{ij} \epsilon_i \epsilon_j^*}{\int_0^\infty \rho_0 u_k u_k^* dz} dz \tag{13}$$

We only detail the calculations for Love waves.
• Love waves.
By using previous expressions for $\mathbf{u}(\mathbf{r}, t)$ (9) and $\epsilon_{ij}(\mathbf{r}, \mathbf{t})$ (10), the various expressions of strain are:

$$\begin{cases} \epsilon_1 &= -i \cos\Psi \sin\Psi \, kW \\ \epsilon_2 &= i \cos\Psi \sin\Psi \, kW \\ \epsilon_3 &= 0 \\ \epsilon_4 &= 1/2 \cos\Psi \, W' \\ \epsilon_5 &= -1/2 \sin\Psi \, W' \\ \epsilon_6 &= 1/2(\cos^2\Psi - \sin^2\Psi) \, kW \end{cases} \tag{14}$$

where $W' = \frac{dW}{dr}$. In table 1, the different terms $n_{ij}c_{ij}\epsilon_i\epsilon_j^*$ are given. We note that when $c_{ij}\epsilon_i\epsilon_j^*$ is a purely imaginary complex, its contribution to $\delta C(k, \Psi)$ is null. When all the contributions are summed, the different terms $\cos^k\Psi \sin^l\Psi$ are such that $k + l$ is even, which is not surprising in the light of the reciprocity principle. Therefore, each term can be developed as a Fourier series in Ψ with only even terms. Finally it is found:

$$\begin{aligned} \delta C_L(k, \Psi) \;\; = \frac{C}{2\omega^2 L_0} \;\; & \int_0^\infty dz \{k^2 W^2 [\frac{1}{8}(c_{11} + c_{22} - 2c_{12} + 4c_{66}] + W'^2 [\frac{1}{2}(c_{44} + c_{55})] \\ & + \cos 2\Psi \, W'^2 [\frac{1}{2}(c_{44} - c_{55})] - \sin 2\Psi \, W'^2 c_{45} \end{aligned}$$

$$- \cos 4\Psi\, k^2 W^2 [\frac{1}{8}(c_{11} + c_{22} - 2c_{12} - 4c_{66})] \qquad (15)$$
$$+ \sin 4\Psi\, k^2 W^2 [\frac{1}{2}(c_{26} - c_{16})]\}$$

In the particular case of a transversely isotropic medium with a vertical symmetry axis (also named radial anisotropic medium), we have: $c_{11} = c_{22} = \delta A$, $c_{33} = \delta C$, $c_{12} = \delta(A - 2N)$, $c_{13} = c_{23} = \delta F$, $c_{44} = c_{55} = \delta L$, $c_{66} = \delta N$ and $c_{14} = c_{24} = c_{15} = c_{25} = c_{16} = c_{26} = 0$. The local azimuthal terms vanish and the previous equation (15) reduces to:

$$\delta C_L(k, \Psi) = \frac{1}{2C_L L_0} \int_0^\infty dz \{W^2 \delta N + \frac{W'^2}{k^2} \delta L\} dz \qquad (16)$$

Therefore, the same expressions as in *Takeuchi and Saito* (1972, p. 268) are found in the case of radial anisotropy. The $0 - \Psi$ term of equation (15) corresponds to the averaging over azimuth Ψ, which provides the equivalent transversely isotropic model with vertical symmetry axis by setting:
$\delta N = \frac{1}{8}(c_{11} + c_{22}) - \frac{1}{4}c_{12} + \frac{1}{2}c_{66}$
$\delta L = \frac{1}{2}(c_{44} + c_{55})$
If we call C_{ij} the elastic coefficients of the total elastic tensor, we can set:
$N = \rho V_{SH}^2 = \frac{1}{8}(C_{11} + C_{22}) - \frac{1}{4}C_{12} + \frac{1}{2}C_{66}$
$L = \rho V_{SV}^2 = \frac{1}{2}(C_{44} + C_{55})$
According to equation (15), the first order perturbation in Love wave phase velocity $\delta C_L(k, \Psi)$ can then be expressed as:

$$\delta C_L(k, \Psi) = \frac{1}{2C_{0_L}(k)} [L_1(k) + L_2(k) \cos 2\Psi + L_3(k) \sin 2\Psi + L_4(k) \cos 4\Psi + L_5(k) \sin 4\Psi \quad (17)$$

where

$$L_0(k) = \int_0^\infty \rho W^2 dz$$
$$L_1(k) = \frac{1}{L_0} \int_0^\infty (W^2 \delta N + \frac{W'^2}{k^2} \delta L) dz$$
$$L_2(k) = \frac{1}{L_0} \int_0^\infty -G_c(\frac{W'^2}{k^2}) dz$$
$$L_3(k) = \frac{1}{L_0} \int_0^\infty -G_s(\frac{W'^2}{k^2}) dz$$
$$L_4(k) = \frac{1}{L_0} \int_0^\infty -E_c.W^2 dz$$
$$L_5(k) = \frac{1}{L_0} \int_0^\infty -E_s.W^2 dz$$

• Rayleigh waves.
The same procedure holds for the local Rayleigh wave phase velocity perturbation δC_R, starting from the displacement given previously (*Montagner and Nataf*, 1986).

$$\delta C_R(k, \Psi) = \frac{1}{2C_{0_R}(k)} [R_1(k) + R_2(k) \cos 2\Psi + R_3(k) \sin 2\Psi + R_4(k) \cos 4\Psi + R_5(k) \sin 4\Psi \quad (18)$$

where

$$
\begin{aligned}
R_0(k) &= \int_0^\infty \rho(U^2+V^2)dz \\
R_1(k) &= \frac{1}{R_0}\int_0^\infty [V^2.\delta A + \frac{U'^2}{k^2}.\delta C + \frac{2U'V}{k}.\delta F + (\frac{V'}{k}-U)^2.\delta L]dz \\
R_2(k) &= \frac{1}{R_0}\int_0^\infty [V^2.B_c + \frac{2U'V}{k}.H_c + (\frac{V'}{k}-U)^2.G_c]dz \\
R_3(k) &= \frac{1}{R_0}\int_0^\infty [V^2.B_s + \frac{2U'V}{k}.H_s + (\frac{V'}{k}-U)^2.G_s]dz \\
R_4(k) &= \frac{1}{R_0}\int_0^\infty E_c.V^2dz \\
R_5(k) &= \frac{1}{R_0}\int_0^\infty E_s.V^2dz
\end{aligned}
$$

The 13 depth-dependent parameters $A, C, F, L, N, B_c, B_s, H_c, H_s, G_c, G_s, E_c, E_s$ are linear combinations of the elastic coefficients C_{ij} and are explicitly given as follows:

Constant term (0 Ψ -azimuthal term: independent of azimuth)

$$
\begin{aligned}
A &= \rho V_{PH}^2 = \tfrac{3}{8}(C_{11}+C_{22}) + \tfrac{1}{4}C_{12} + \tfrac{1}{2}C_{66} \\
C &= \rho V_{PV}^2 = C_{33} \\
F &= \tfrac{1}{2}(C_{13}+C_{23}) \\
L &= \rho V_{SV}^2 = \tfrac{1}{2}(C_{44}+C_{55}) \\
N &= \rho V_{SH}^2 = \tfrac{1}{8}(C_{11}+C_{22}) - \tfrac{1}{4}C_{12} + \tfrac{1}{2}C_{66}
\end{aligned}
$$

2 Ψ -azimuthal term:

$\cos 2\Psi$	$\sin 2\Psi$
$B_c = \frac{1}{2}(C_{11}-C_{22})$	$B_s = C_{16}+C_{26}$
$G_c = \frac{1}{2}(C_{55}-C_{44})$	$G_s = C_{54}$
$H_c = \frac{1}{2}(C_{13}-C_{23})$	$H_s = C_{36}$

4 Ψ -azimuthal term:

$\cos 4\Psi$	$\sin 4\Psi$
$E_c = \frac{1}{8}(C_{11}+C_{22}) - \frac{1}{4}C_{12} - \frac{1}{2}C_{66}$	$E_s = \frac{1}{2}(C_{16}-C_{26})$

where indices 1 and 2 refer to horizontal coordinates (1: North; 2: East) and index 3 refers to vertical coordinate. ρ is the density, V_{PH}, V_{PV} are respectively horizontal and vertical P-wave velocities, V_{SH}, V_{SV} horizontal and vertical S-wave velocities. We must bear in mind that A, C, L, N anisotropic parameters can be retrieved from measurements of the P- and S- wave velocities propagating perpendicular or parallel to the axis of symmetry. Some of the previous combinations were already derived in the expressions that describe the azimuthal dependence of body waves (see *Crampin et al.* (1984) for example) in a weakly anisotropic medium.

$$\rho V_P^2 = A + B_c \cos 2\Psi + B_s \sin 2\Psi + E_c \cos 4\Psi + E_s \sin 4\Psi$$

$$\rho V_{SP}^2 = N - E_c \cos 4\Psi - E_s \sin 4\Psi$$

$$\rho V_{SR}^2 = L + G_c \cos 2\Psi + G_s \sin 2\Psi$$

Therefore, the equations (17) and (18) define the forward problem in the framework of a first order perturbation theory. We will see in the next section how to solve the inverse problem. That means that, ideally, surface waves have the ability for providing 13 elastic parameters, which emphasizes the enormous potential of surface waves in terms of geodynamical and petrological implications. However, from a practical point of view, data do not have the resolving power for inverting for so many parameters. *Montagner and Anderson* (1989a) proposed to use constraints from petrology in order to reduce the parameter space. Actually, they found that some of these parameters display large correlations independent of the petrological model used. Two extreme models were used to derive these correlations, the pyrolite model (*Ringwood*, 1975) and the piclogite model (*Anderson and Bass*, 1984, 1986; *Bass and Anderson*, 1984). In the inversion process, the smallest correlations between parameters of both models are kept. This approach was already followed by *Montagner and Anderson* (1989b) to derive an average reference earth model. These simple linear combinations of the elastic tensor components were first displayed by *Montagner and Nataf* (1986) and they enable to describe in a simple way the two seismically observable effects of anisotropy on surface waves, the "polarization" anisotropy (*Schlue and Knopoff*, 1977) and the azimuthal anisotropy (*Forsyth*, 1975).
In conclusion, the 0-Ψ term corresponds to the average over all azimuths and involves 5 independent parameters, A, C, F, L, N, which express the equivalent transverse isotropic medium with vertical symmetry axis (more simply named radial anisotropy). The other azimuthal terms (2-Ψ and 4-Ψ) depend on 4 groups of 2 parameters, B, G, H, E respectively describing the azimuthal variation of A, L, F, N.
The other important point in these expressions is that they provide the partial derivatives for the radial and azimuthal anisotropy of surface waves. These partial derivatives of the different azimuthal terms with respect to the elastic parameters can be easily calculated by using a radial anisotropic reference Earth model, such as *PREM* (*Dziewonski and Anderson*, 1981). The corresponding kernels and their variation at depth are detailed and discussed for the fundamental mode in *Montagner and Nataf* (1986). The partial derivatives of the eigenperiod ${}_0T_l$ with respect to parameter p, $\frac{p}{T}\frac{\partial T}{\partial p}$ can easily be converted into phase velocity partial derivatives by using:

$$\frac{p}{C}(\frac{\partial C}{\partial p})_T = -\frac{C}{U}\frac{p}{T}(\frac{\partial T}{\partial p})_k$$

For example, the parameters G_c and G_c have the same kernel as parameter L (related to V_{SV}) as shown by comparing R_1, R_2 and R_3 . The calculation of kernels shows that Love waves are almost insensitive to V_{SV} and Rayleigh waves to V_{SH}. Rayleigh waves are the most sensitive to SV-waves. However, as pointed out by *Anderson and Dziewonski* (1982), the influence of P-waves (through parameters A and C) can be very large in an anisotropic medium. The influence of density is also very large for Love and Rayleigh waves, but as shown by *Takeuchi and Saito* (1972), it is largely decreased when seismic velocities are inverted for, instead of elastic moduli and density. We will now show how to implement such a theory from a practical point of view, and how to design a tomographic technique in order to invert for the 13 different anisotropic parameters, which arise as well in the plane case as in the spherical case.

Table 1: Calculation of the various $c_{ij}\epsilon_i\epsilon_j$ for Love waves, with the simplified index notation. $\alpha = \cos\Psi$; $\beta = \sin\Psi$

n	ij	$c_{ij}\epsilon_i\epsilon_j$
1	11	$c_{11}\alpha^2\beta^2.k^2W^2$
1	22	$c_{22}\alpha^2\beta^2.k^2W^2$
1	33	0
2	12	$-c_{12}\alpha^2\beta^2.k^2W^2$
2	13	0
2	23	0
2	24	0
4	14	$c_{14}(-i\alpha^2\beta).\frac{kWW'}{2}$
4	15	$c_{15}(i\alpha^2\beta).\frac{kWW'}{2}$
4	16	$c_{16}(-\alpha\beta)(\alpha^2-\beta^2).\frac{k^2W^2}{2}$
4	24	$c_{24}(-i\alpha^2\beta).\frac{kWW'}{2}$
4	25	$c_{25}(-i\alpha\beta^2).\frac{kWW'}{2}$.
4	26	$c_{26}(\alpha\beta)(\alpha^2-\beta^2).\frac{k^2W^2}{2}$
4	34	0
4	35	0
4	36	0
4	44	$c_{44}\alpha^2.\frac{W'^2}{4}$
8	45	$c_{45}(-\alpha\beta).\frac{W'^2}{4}$
8	46	$c_{46}(-i\alpha)(\alpha^2-\beta^2).\frac{kWW'}{2}$
4	55	$c_{55}\beta^2.\frac{W'^2}{4}$
8	56	$c_{56}(i\beta)(\alpha^2-\beta^2).\frac{kWW'}{2}$
4	66	$c_{66}(\alpha^2-\beta^2).\frac{k^2W^2}{4}$

4 Tomography of anisotropy

Tomography is a generic term used by seismologist for naming a technique able to image the 3D structure of an object. The object is usually illuminated by a large number of ray and its structure is recovered by an inversion procedure. A good description of this object means that we can find its correct location in space and its physical properties (amplitude and spectral content). A tomographic technique necessitates to solve at the same time, a forward problem and an inverse problem. By using the results of the previous section, we will successively consider how to set the forward problem, and how it is used to calculate the partial derivatives of data with respect to parameters, for retrieving a set of parameters.

4.1 Forward problem

We have first to define the data space **d** and the parameter space **p**. We assume that a functional **g** relating **d** and **p** can be found such that:
$\mathbf{d} = \mathbf{g}(\mathbf{p})$, where **d** is the set of data (which samples the data space), and **p** the set of parameters.
Data Space: d
The basic dataset is made of seismograms $\mathbf{u}(t)$. We can try to directly match the waveform in the time domain, or we can work in the Fourier domain, by separating phase and amplitude on each component:

$$u_i(t) = \int_{\infty}^{\infty} A_i(\omega) e^{i(\omega t - \phi_i)} d\omega$$

The approach consisting in fitting seismic waveform is quite general but, from a practical point of view, it does not necessarily correspond to the simplest choice. In a heterogeneous medium, the calculation of amplitude effects makes it necessary to calculate the coupling between different multiplets, which is very time consuming. When working in Fourier domain, we can consider different time windows and separately match the phase of different seismic trains, body waves and surface waves. We showed in Figure 9 an example of data seismogram and synthetic seismograms obtained by normal mode summation with the different higher modes. The fundamental wavetrain is well separated from other modes at large epicentral distance. The part of the seismogram corresponding to higher modes is more complex and shows a mixing of these modes in the time domain. Therefore, from a practical point of view, the fitting of the fundamental mode wavetrain will not cause any problem and has been widely used in global mantle tomography.
The use of higher mode wavetrain and the separation of overtones is much more difficult. The first attempts were performed by *Nolet* (1975), *Cara* (1978), *Okal and Bong-Jo* (1985) and *Dost* (1990) by applying a spatial filtering method. Different techniques based on waveform inversion of fundamental and higher-mode surface waves were also designed in the following years (*Lerner-Lam*, 1983; *Nolet*, 1990; *Lévêque et al.*, 1991). Unfortunately, all these techniques can only be applied to areas where dense arrays of seismic stations are present, i.e. in North America and Europe. By using a set of seismograms either recorded in one station but corresponding to several earthquakes located in a small source area, *Stutzmann and Montagner* (1993) showed how to separate the different higher modes. A similar approach was recently followd by *Van Heijst and Woodhouse* (1998). This technique might be easily applied as well, to seismograms originating from one seismic source recorded in an array of stations. Since it is necessary to fit

higher mode wave packet, it is shown that it is necessary to recalculate the eigenfunctions at each iteration of the inversion process. We only detail in this paper the technique which was designed for fitting the fundamental mode wavetrain and the reader is referred to *Stutzmann and Montagner* (1993, 1994) and *Van Heijst and Woodhouse* (1998) for recovering the higher mode dispersion properties.

We take advantage of the fact that, according to the Fermat's principle, the phase velocity perturbation is only dependent to second order on path perturbations, whereas amplitude perturbation are dependent, at first order, to these perturbations, which implies that the eigenfunctions must be recalculated at each iteration. Therefore, the phase is a more robust observable than the amplitude. The amplitude $A(\omega)$ depends in a complex manner upon seismic moment tensor, attenuation, scattering, focusing effects, station calibration and near-receiver structure whereas the phase $\phi(\omega)$ is readily related to lateral heterogeneities of seismic velocity and anisotropic parameters. The dataset that we will consider, is composed of propagation times (or phase velocity measurements for surface waves) along paths: $\mathbf{d} = \{\frac{\Delta}{c(T)}\}$.

The second important ingredient in any inverse problem is the structure of the data space. It is expressed through its covariance function (continuous case) or covariance matrix (discrete case) of data C_d. When data d_i are independent, C_d is diagonal and its elements are the square of the errors on data σ_{d_i}.

On the other hand, the phase of a seismogram at time t is decomposed as follows: $\phi = \mathbf{k}.\mathbf{r} + \phi'_0$, where $\mathbf{k}$ is the wave vector, ϕ'_0 is the initial phase which is the sum of several terms: $\phi_0 = \phi_0 + \phi_S + \phi_I$, ϕ_S is the initial source phase, ϕ_0 is related to the number of polar phase shifts, ϕ_I is the instrumental phase. ϕ can be measured on seismograms by Fourier transform. We usually assume that ϕ_S is correctly given by the centroid moment tensor solution. For a path between epicenter S and receiver R with an epicentral distance Δ, the phase ϕ is given by:

$$\phi = \frac{\omega\Delta}{C_{obs}} + \phi_0 + \phi_S + \phi_I \tag{19}$$

or

$$\phi - \phi'_0 = \frac{\omega\Delta}{C_{obs}(T)} = \int_E^R \frac{\omega ds}{C(T,\theta,\phi)} \tag{20}$$

Where the integral is understood between the epicenter E and the receiver R. Following the results of the previous section, different approximations are implicitly made when using this expression of the phase:

- large angular order $\ell \gg 1$, but not too large (scattering problems). From a practical point of view, that means that measurements are performed in the period range 50s. $< T <$ 300s.
- geometrical optics approximation: If λ is the wavelength of the surface wave at period T, and Λ_S the spatial wavelength of heterogeneity: $\Lambda_S \gg \lambda = CT \Rightarrow \Lambda_S \gtrsim 2000km$.
- slight anisotropy and heterogeneity: $\frac{\delta C}{C} \ll 1$. According to *Smith and Dahlen* (1973) for the plane case (equations 18 and 19), the local phase velocity can be decomposed as a Fourier series of the azimuth Ψ:

$$\frac{\delta C(T,\theta,\phi)}{C(T,\theta,\phi)} = A_0 + A_1 \cos 2\Psi + A_2 \sin 2\Psi + A_3 \cos 4\Psi + A_4 \sin 4\Psi \tag{21}$$

Each azimuthal term $A_i(T,\theta,\phi)$ can be related to the set of parameters p_i (density + 13 elastic parameters).

$$\frac{\Delta}{C_{obs}(T)} - \frac{\Delta}{C_0(T)} = -\sum_{j=0}^{2}\sum_{i=1}^{13} \int_E^R \frac{ds}{C_0} \int_0^a \left[\left(\frac{p_i}{C}\frac{\partial C}{\partial p_i} \right)_j \frac{\delta p_i(\vec{r})}{p_i} \cos(2j\Psi) + \left(\frac{p_i}{C}\frac{\partial C}{\partial p_i} \right)_j \frac{\delta p_i(\vec{r})}{p_i} \sin(2j\Psi) \right] \frac{dz}{\Delta h} \qquad (22)$$

However, many terms in equation (22) are equal to zero since all parameters are not present in each azimuthal term. Following the approach of *Snieder* (1996), the approximations that have been made, mean that the perturbed medium is at the same time smooth and weak.

Parameter space: p(r)

It is quite important to thoroughly think of the structure of the parameter space. First of all, it is necessary to define which parameters are required to explain our dataset, and how many **physical parameters** can be effectively inverted for, in the framework of the theory that is considered. For example, if the Earth is assumed to be elastic, laterally heterogeneous but isotropic, only 3 independent physical parameters, V_P, V_S and density ρ (or the elastic moduli λ, $\mu + \rho$) can be inverted for. In a transversely isotropic medium with a vertical symmetry axis (*Anderson*, 1961; *Takeuchi and Saito*, 1972), the number of independent physical parameters is now 6 (5 elastic moduli + density). In the most general case of a weak anisotropy, 14 physical parameters (13 combinations of elastic moduli + density) can be inverted for. Therefore, the number of "physical" parameters p_i is dependent on the underlying theory which is used for explaining the dataset.

Once the number of "physical" independent parameters is defined, we must be able to define how many "**spatial**" (or geographical) parameters are required to describe the 3D distributions $p_i(r, \theta, \phi)$. That is a difficult problem because the number of "spatial" parameters which can be reliably retrieved from the dataset is not necessarily sufficient to provide a correct description of $p_i(r, \theta, \phi)$. The correct description of $p_i(r, \theta, \phi)$ is dependent on its spectral content: For example, if $p_i(r, \theta, \phi)$ is characterized by very large wavelengths, only a small number of spatial parameters is necessary, but if $p_i(r, \theta, \phi)$ presents very small scale features, the number of spatial parameters will be very large. In any case, it is necessary to assess the range of possible variations for $p_i(r, \theta, \phi)$ in order to provide some bounds on the parameter space. This is done through a covariance function of parameters in the continuous case (or a covariance matrix for the discrete case). These *a priori* constraints can be provided by other fields in geoscience, geology, mineralogy, numerical modeling...

Consequently, a tomographic technique must not be restricted to the inversion of parameters $\mathbf{p} = \{p_i(r, \theta, \phi)\}$ that are searched for, but must include the calculation of the final covariance function (or matrix) of parameters C_p. That means that the retrieval of parameters is contingent to the resolution and the errors of the final parameters and is largely dependent on the resolving power of data (*Backus and Gilbert*, 1967, 1968, 1970).

Finally, the functional $\mathbf{g}$ which expresses the theory relating the data space to the parameter space is also subject to uncertainty. In order to be completely consistent, it should be necessary to be able to define the domain of validity of the theory and to assess the error σ_T associated with the theory. *Tarantola and Valette* (1982) showed that the error σ_T is simply added to the error on data σ_d.

4.2 Inverse problem

The equation (22) expressing the first order perturbation theory of the forward problem in the linear case, can be simply written:

$$\mathbf{d} = \mathbf{G}\mathbf{p}$$

where G is a matrix (or a linear operator) composed of Fréchet derivatives of d with respect to p, which has the dimensions $n_d \times n_p$ (number of data $\times$ number of parameters). This matrix usually is not square and many different techniques in the past have been used for inverting G. In any case, the inverse problem will consist in finding an inverse for the functional $\mathbf{g}$, that we will write $\tilde{\mathbf{g}}^{-1}$, notwithstanding the way it is obtained, such that:

$$\mathbf{p} = \tilde{\mathbf{g}}^{-1}(\mathbf{d})$$

Different strategies can be followed to invert for the 3D-models $\mathbf{p}(\mathbf{r})$, because the size of the inverse problem is usually enormous in practical applications. For the example of mantle tomography, a *minimum* parameter space will be composed of 13 (+density) physical parameters multiplied by 30 layers, in dividing the mantle into 30 independent layers. If geographical distributions of parameters are searched for up to degree 36 (lateral resolution around 1000km), that implies $\approx 600,000$ parameters. The problem is still very hard to handle from a computational point of view. A simple approach for solving this problem consists in dividing the inversion procedure into 2 steps (see *Montagner*, 1996) for a description of this approach).
To solve the inverse problem, different algorithms can be used. The most general algorithm has been derived by *Tarantola and Valette* (1982):

$$\begin{aligned} \mathbf{p} - \mathbf{p_0} &= (G^t C_d^{-1} G + C_{p_0}^{-1})^{-1} G^t C_d^{-1} (\mathbf{d} - \mathbf{g}(\mathbf{p}) + G(\mathbf{p} - \mathbf{p_0})) \\ &= C_{p_0} G^t (C_d + G C_{p_0} G^t)^{-1} (\mathbf{d} - \mathbf{g}(\mathbf{p}) + G(\mathbf{p} - \mathbf{p_0})) \end{aligned} \tag{23}$$

where C_d is the covariance matrix of data, C_{p_0} the covariance function of parameters $\mathbf{p}$, and G is the Frechet derivative of the operator $\mathbf{g}$ at point $\mathbf{p}(\mathbf{r})$. This algorithm can be made more explicit by writing it in its integral form:

$$\mathbf{p}(\mathbf{r}) = \mathbf{p_0}(\mathbf{r}) + \sum_i \sum_j \int_V d\mathbf{r}' C_{p_0}(\mathbf{r}, \mathbf{r}') G_i(\mathbf{r}') (S^{-1})_{ij} F_j \tag{24}$$

with $S_{ij} = C_{d_{ij}} + \int_V d\mathbf{r_1} d\mathbf{r_2}\, G_i(\mathbf{r_1}) C_{p_0}(\mathbf{r_1}, \mathbf{r_2})\, G_j(\mathbf{r_2})$
and $F_j = d_j - g_j(\mathbf{p} + \int_V d\mathbf{r}"\, G_j(\mathbf{r}")(\mathbf{p}(\mathbf{r}") - \mathbf{p_0}(\mathbf{r}"))$
This algorithm can be iterated and enables to solve slightly non-linear problems, which is the case for the inversion at depth. In case of a large dataset, *Montagner and Tanimoto* (1990) showed how to handle the inverse problem by making a series expansion of the inverse of matrix S. One of the advantage of this technique is that it can be applied indifferently to regional studies or global studies. In case of imperfect spatial coverage of the area under investigation, it does not display ringing phenomena commonly observed when a spherical harmonics expansion is used (*Tanimoto*, 1985).
The *a posteriori* covariance function is given by:

$$C_p = C_{p_0} - C_{p_0} G^T (C_d + G C_{p_0} G^T)^{-1} G C_{p_0} = (G^T C_d^{-1} G + C_{p_0}^{-1})^{-1} \tag{25}$$

The choice of the parameterization is also very important and different possibilities can be considered:

• Discrete basis of functions: For a global study, the natural basis is composed of the spherical harmonics for the horizontal variations. For the radial variations, polynomial expansions can be used (see for example *Dziewonski and Woodhouse*, (1987) for Tshebyshev polynomials). Another possibility is to divide the Earth into cells of various size according to the resolution one can expect from the path coverage. The cell decomposition is valid as well for global investigations as for regional studies.

• Continuous function $\mathbf{p}(\mathbf{r})$. In that case, we directly invert for the function. However, the number of parameters is infinite and it is necessary to define a covariance function of parameters $C_{p_0}(\mathbf{r}, \mathbf{r}')$. For the horizontal variations, we can use a Von Mises distribution (*Fisher*, 1953; *Montagner*, 1986b) for initial parameters $\mathbf{p_0}(\mathbf{r})$:

$$C_{p_0}(\mathbf{r}, \mathbf{r}') = \sigma_p(\mathbf{r})\sigma_p(\mathbf{r}') \exp \frac{\cos \Delta_{\mathbf{r}\mathbf{r}'} - 1}{L_{cor}^2}$$

where L_{cor} is the correlation length which will define the smoothness of the final model. This kind of distribution is well suited for studies on a sphere and is asymptotically equivalent to a Gaussian distribution when $L_{cor} \ll a$ (a radius of the Earth). When different azimuthal terms distributions are searched for, it is possible to define cross-correlated covariance functions of parameters $C_{p_i,p_j}(\mathbf{r}, \mathbf{r}')$, but it can be assumed that the different terms of the Fourier expansion in azimuth correspond to orthogonal functions, so the cross-correlated terms outside the diagonal can be taken equal to zero.

For the inversion at depth, since the number of physical parameters is very large, it is difficult to assume that physical parameters are uncorrelated. Then, the different terms of the covariance function C_p between parameters p_1 and p_2 at radii r_i and r_j can be defined as follows:

$$C_{p_1,p_2}(r_i, r_j) = \sigma_{p_1}\sigma_{p_2}\zeta_{p_1,p_2} e^{\frac{(r_i - r_j)^2}{2L_{r_i}L_{r_j}}} \tag{26}$$

Where ζ_{p_1,p_2} is the correlation between physical parameters p_1 and p_2 inferred for instance from different petrological models (*Montagner and Anderson*, 1989a) and L_{r_i}, L_{r_j} are the radial correlation lengths which enable to smooth the inverse model. The resolution R of parameters can be calculated as well. It corresponds to the impulsive response of the system:

$$\mathbf{p} = \tilde{\mathbf{g}}^{-1}\mathbf{d} = \tilde{\mathbf{g}}^{-1}\mathbf{g}\,\mathbf{p}' = R\,\mathbf{p}'$$

If the inverse problem is perfectly solved, R is the identity function or matrix. However, the following expression of resolution is only valid in the linear case (*Montagner and Jobert*, 1981):

$$R = C_{p_0}G^T(C_d + GC_{p_0}G^T)^{-1}G = (G^TC_dG + C_{p_0})^{-1}G^TC_d^{-1}G \tag{27}$$

It is interesting to note, that the local resolution of parameters is imposed by both the correlation length and the path coverage, contrarily to the *Backus-Gilbert* (1967, 1968) approach, which primarily depends on the path coverage. But the effect of a damping factor in order to smooth the solution, is equivalent to the introduction of a simple covariance function on parameters weighted by the errors on data (*Ho-Liu et al.*, 1989). When the correlation length is chosen very small, the algorithms of *Backus-Gilbert* (1968, 1970) and *Tarantola and Valette* (1982) are quite equivalent.

By considering the *a posteriori* covariance function and the resolution, it is possible to assess the reliability of the hypotheses made about the independence of parameters. For example *Tanimoto and Anderson* (1985) and *Montagner and Jobert* (1988) showed that there is a trade-off between azimuthal terms and constant term in case of a poor azimuthal coverage. For the inversion at depth *Nataf et al.* (1986) display as well the trade-off between physical parameters V_{PH}, V_{SV}, ξ, ϕ and η when only Rayleigh and Love wave $0 - \Psi$-terms are used in the inversion process.

4.3 Practical implementation.

The complete anisotropic tomographic procedure has been implemented for making different regional and global studies. From petrological and mineralogical considerations, *Montagner and Nataf* (1988) and *Montagner and Anderson* (1989a,b) showed that the predominant terms of phase velocity azimuthal expansion are the 0-Ψ and 2-Ψ for Rayleigh waves, and 0-Ψ and 4-Ψ for Love waves. *Montagner and Nataf* (1988) showed that the best resolved parameters are $L = \rho V_{SV}^2$, $N = \rho V_{SH}^2$ and G_c, G_s, E_c, E_s which respectively express the azimuthal variations of V_{SV} and V_{SH}.
Another important point emphasized by *Montagner and Jobert* (1988) and *Montagner and Tanimoto* (1991) is the importance of shallow layers (oceanic - continental crusts, bathymetry - topography, sedimentary thicknesses...) on phase velocity. In order to avoid the deep structure to be biased by an improper account of shallow layers, it is necessary to correct phase velocity measurements along each path. This correction is not negligible, and contrarily to the common belief, it tends to increase the amplitude of lateral heterogeneities below the crust.
This technique has made it possible to simultaneously explain the "Rayleigh-Love discrepancy" and the azimuthal anisotropy, firstly displayed in the Nazca plate by *Forsyth* (1975). However, the main limitation of this technique applied to the fundamental mode of surface waves is that the radial resolution is limited to the first 500km of the upper mantle. In order to go further, it is necessary to use seismic waves sensitive to deeper structure. Multiple reflected S-waves and surface wave overtones are good candidates for doing that. The first approach using body waves obtained by normal mode summation was followed by *Nolet and Kennett* (1978), *Tanimoto* (1990), *Su and Dziewonski* (1991, 1992) and *Woodward and Masters* (1991a,b) and many others in the nineties. On the other hand, *Stutzmann and Montagner* (1993, 1994) showed how to generalize the 2-step tomographic technique to higher modes for retrieving the global structure down to the CMB (Core-Mantle Boundary).

4.4 Geophysical applications

The number of applications of seismic tomography is very large. Seismic tomography is the most efficient approach to visualize, at the same time, seismic velocities and anisotropy heterogeneities, which can, in turn be related to temperature, flow directions and petrological anomalies. Therefore, the different fields interested in seismic tomography are geodynamics, gravimetry, geochemistry and tectonics. We will briefly review what kind of information can be provided by tomographic models.

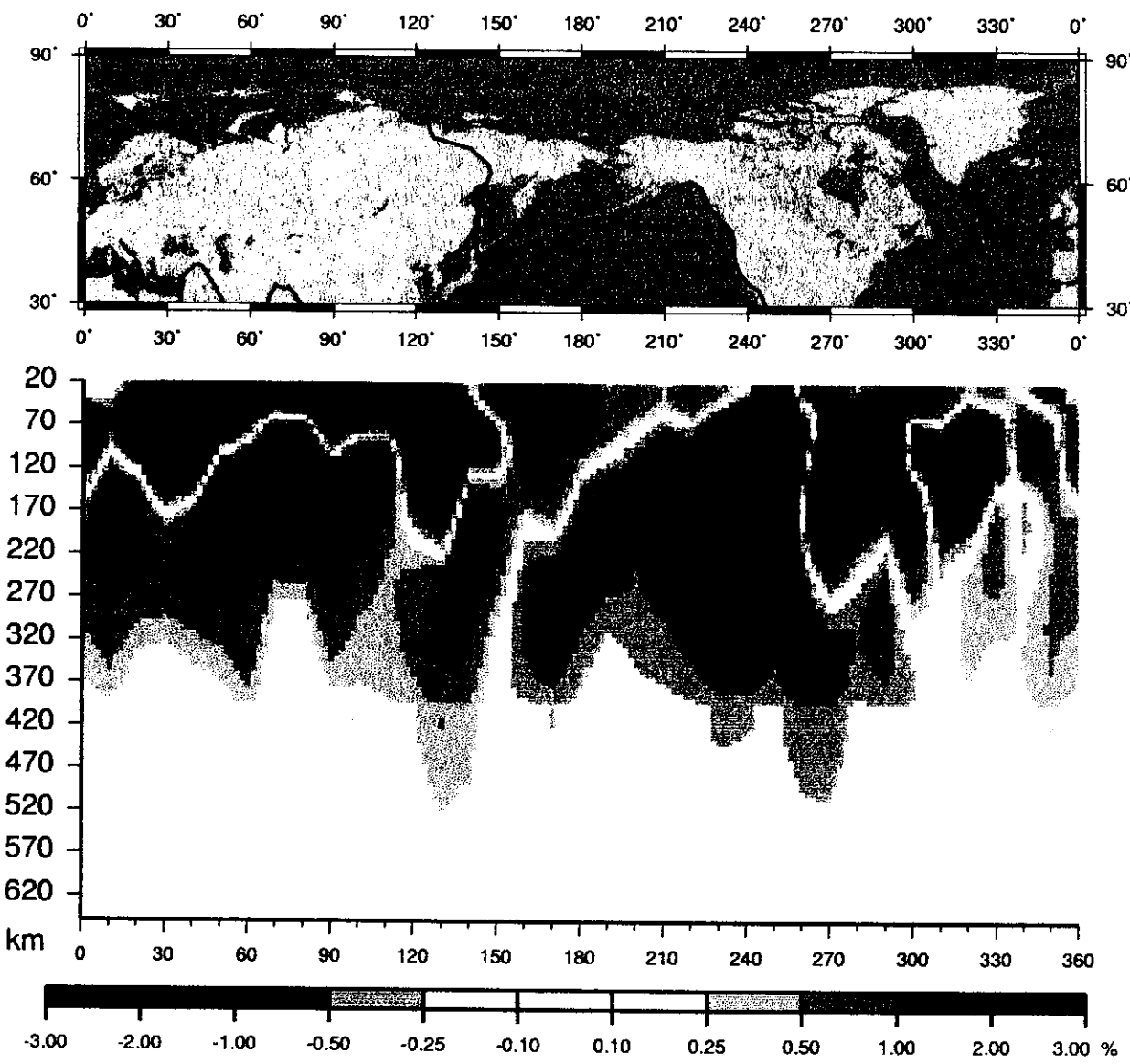

Figure 11: Two examples of tomographic images obtained by simultaneous inversion of isotropic parameters and anisotropic parameters (Model AUM of *Montagner and Tanimoto*, 1991). Cross-sections are taken at 30° North.
Top: SV-wave velocity. Since most velocity anomalies reflect temperature anomalies, the color scale reflects hot and cold regions at this depth. The isolines are separated by 1%.
Bottom: ξ. In terms of interpretation, warm colors reflect the radial or sub-radial flow (upwelling or downwelling), and cold colors are related to horizontal or sub-horizontal flow.

Xi Anisotropy: Radial cross-section 30 deg. AUM model (Montagner and Tanimoto, 1991)

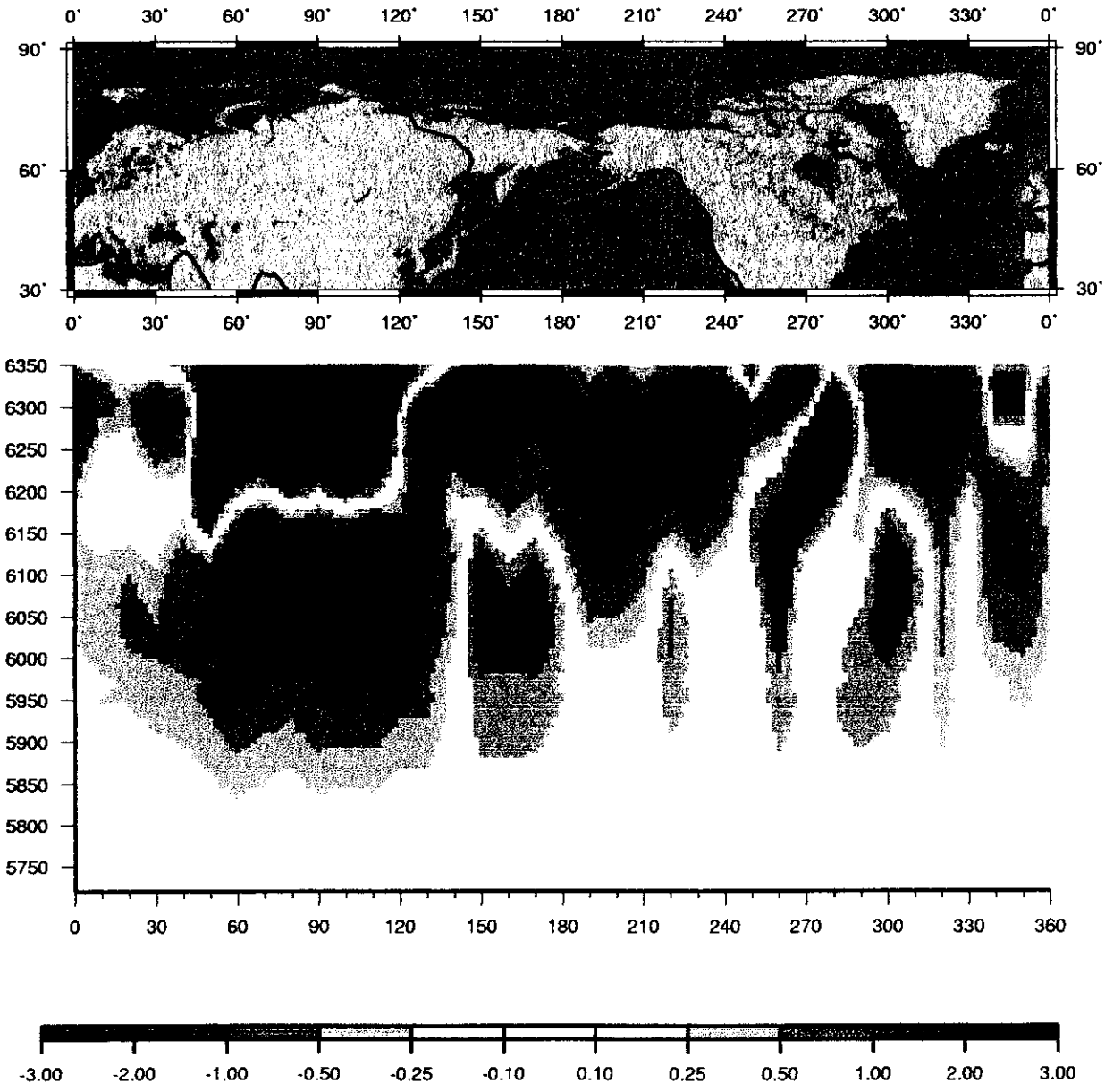

• **Geodynamics**

The most popular application of large-scale tomographic models is the understanding of mantle convection. Seismic velocity anomalies can be converted, under some assumptions, into temperature anomalies, density anomalies but also into chemical or mineralogical heterogeneities. Since *Hager et al.* (1985), numerous studies have been devoted to the correlation between 3D seismic velocity structure, the dynamic topography, the geoid and the gravimetric anomalies. The main advantage of anisotropy measurements is to provide the principal directions of the strain rate tensor, which are related to flow directions (*Anderson*, 1989). Therefore, the simultaneous use of seismic velocity and anisotropy heterogeneities enables to spatially locate temperature and petrological heterogeneities, and their directions of flow. *Montagner and Nataf* (1988) present a method for inverting a local symmetry axis. *Montagner and Jobert* (1988), and *Hadiouche et al.* (1989) have been able to plot the 3D-distribution of this axis, respectively in the Indian ocean and in Africa. *Montagner* (1994) presents what can seismic global tomographic models tell us about mantle convection and what robust features can be drawn from the different available models.

Most tomographic models agree, that down to about 300km, the deep structure is closely related to plate tectonics and continental distribution. Simultaneously to the SV-wave velocity, 3 anisotropic paramaters are well resolved: the ξ parameter expresses the relative variation of V_{SV} versus V_{SH}, providing the tendency for the flow to be rather radial or horizontal, and the G, Ψ_G parameters express the azimuthal variation of V_{SV}. Figure 11 presents 2 vertical cross-sections for V_{SV} (figure 11a) and ξ (figure 11b) from model AUM (*Montagner and Tanimoto*, 1991), which illustrates the most robust features of the upper mantle models published so far. In the upper depth range (down to 200km), plate boundaries are slow: ridges and back-arc areas are slow, shields are fast and seismic velocity in oceanic areas is increasing with the age of the seafloor. The comparison between figure 11a and 11b, shows that both maps are poorly correlated. That suggests that they are conveying independent, but complementary information.

Figures 12 display horizontal cross-sections at 200km depth for V_{SV}, ξ and G parameter. The amplitude of SV-wave azimuthal anisotropy (G parameter) presents an average value of about 2% below oceanic areas (Figure 12c). It can be noted a good correlation between seismic azimuthal anisotropy and plate velocity directions given by *Minster and Jordan* (1978). At the stage of interpretation in terms of mantle convection, it is important to consider these 3 maps simultaneously. For example, the existence of a maximum in radial anisotropy in the depth range 200-300km below shields suggest that the root of shields is located in this depth range, whereas some fast velocity anomalies are still present below some continents (*Montagner*, 1998; *Babuska et al.*, 1998). As depth is increasing, the amplitude of heterogeneities is rapidly decreasing, some trends tend to vanish, and some distinctive features come up: Fast ridges are still slow but slow ridges are hardly visible and back-arc regions are no longer systematically slow. Large portions of fast ridges are offset with respect to their surface signatures. Below 300km of depth, a high velocity body below western Pacific can be related to subducting slabs.

Figure 12: Two examples of tomographic images obtained by simultaneous inversion of isotropic parameters and anisotropic parameters (Model AUM of *Montagner and Tanimoto*, 1991).
Top: SV-wave velocity at 200km depth.
Middle: $\xi = N/L - 1$ radial anisotropy at 200km depth.
Bottom: SV-wave azimuthal anisotropy expressed by parameter G at 200km. It can be noted a good correlation between directions of maximum velocity and tectonic plate velocity directions.

Vs AUM model for =200 km

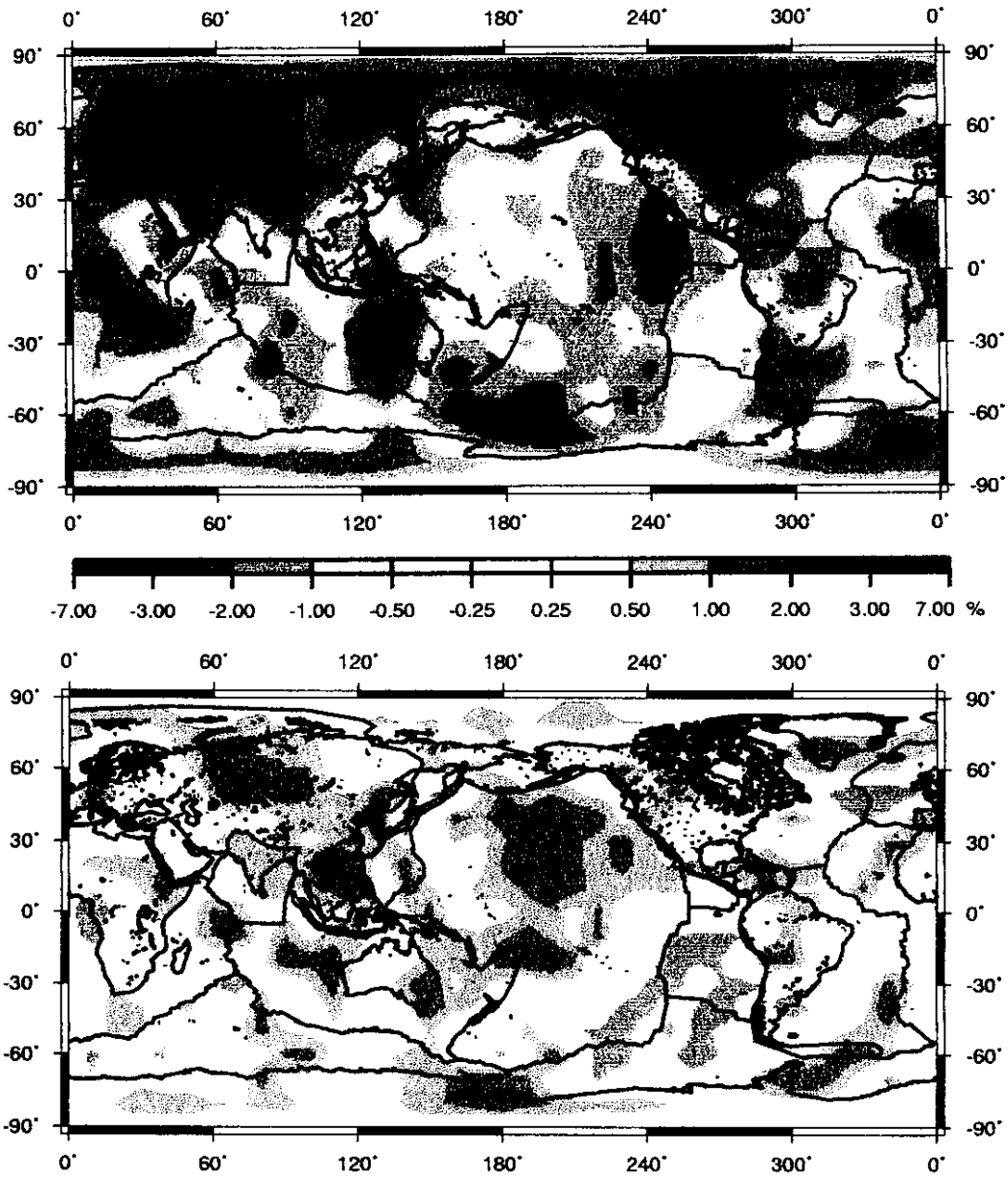

Vsv Azimuthal Anisotropy at 200km (G-parameter)
200 AMAX= 3.8

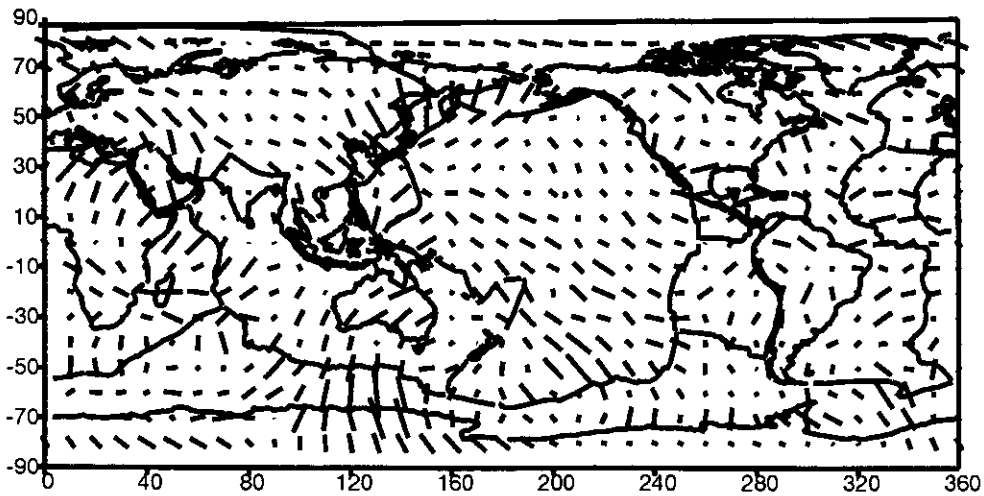

In order to enable a quantitative comparison with other geophysical observables, tomographic models are usually expanded in spherical harmonics according to:

$$f(r,\theta,\phi) = \sum_{l=0}^{l_{max}} \sum_{m=-l}^{m=l} a_l^m(r) Y_\ell^m(\theta,\phi)$$

where r, θ, ϕ are the spherical coordinates at $\mathbf{r}$ and $Y_\ell^m(\theta,\phi)$ is the spherical harmonic of angular order ℓ and azimuthal order m. Another important parameter is the power spectrum $P_l(r)$, which provides the amplitude of anomalies at different degrees ℓ at different depths r.
In the first 300-400km of depth, the power spectrum regularly decreases with decreasing wavelength. This decrease can be described by a l^{-1} law (*Tanimoto*, 1990). At greater depth, in the transition zone, degree 2 (*Masters et al.*, 1982) and to a less extent, degree 6 distributions become predominant. It is also found that degree 4 of radial anisotropy (*Roult et al.*, 1990; *Montagner and Tanimoto*, 1991) is the most important degree for this parameter. A simple flow pattern with 2 upgoing and 2 downgoing large-scale flows can be invoked to simply explain the predominance of these different degrees (*Montagner and Romanowicz*, 1993). Therefore, below the apparent complexity of plate tectonics, mantle convection is surprisingly simply organized in the transition zone. Between 400 and 1000km, these large-scale flows are not independent from the circulation in the first 400km but are related to the most tectonically active zones (fast ridges and slabs). This simple flow pattern, usually called degree 2 pattern, is also present in the lower mantle but offset with respect to the one in the transition zone. However, the nature of the power spectrum in the lower mantle is still subject of controversy (*Su and Dziewonski*, 1992).
It is also suggested that tomographic degree 6 is not independent of the deep degree 2 but might be a consequence of this simple flow pattern (*Cazenave et al.*, 1989; *Montagner and Romanowicz*, 1993). Since the hotspot distribution displays a large degree 6 (*Richards and Hager*, 1988), the good correlation between hotspot and seismic degrees 6 favors an origin of most of hotspots in the transition zone. However, 2 superplumes in Central Pacific and Central Africa have their origin in the lower mantle. As shown by *Vinnik et al.* (1997) in the Pacific Ocean, these superplumes might feed other plumes, by a branching effect in the transition zone. The same branching effect was evidenced below the lithosphere in Africa (*Hadiouche et al.*, 1989), where the plume below the Horn of Africa is feeding other small plumes in western Africa. However, a complete understanding of the structure of plumes is still missing. The application of new techniques based on the scattering effects of plumes on surface waves (*Capdeville et al.*, 1999) or body waves (*Ying and Nataf*, 1998) should provide some answers to this difficult issue.
There seems to be a global decoupling in the mantle, between upper structure and lower structure around 800-1000km (*Montagner*, 1994), or around 1700km (*van der Hilst and Karason*, 1999), but there is some radial continuity of seismic velocity in the whole mantle in some places where slabs are present, and for 2 superplumes in central Pacific and Africa. All these issues are still subject of vigorous debate and call for more reliable tomographic models in the transition zone. However, there is a good consensus to say that the mantle cannot be divided into independent convecting cells but is characterized by imbricated convection, where different scales coexist and where exchange of matter is possible.
• Other applications in Geochemistry, Tectonics and Petrology

There are some attempts to make a quantitative comparison between the major-element chemistry of basalts erupted at mid-ocean ridges (MORB) and upper mantle shear wave velocity (*Humler et al.*, 1993). The main advantage of this approach is that it can provide a way for locating at depth the reservoirs displayed by geochemists. For instance, it is found a strong correlation between basalt chemistry and seismic velocity at depths 100-170km, for lateral wavelengths of 1,000- 2,400km, supporting a common thermal origin for the 2 types of signal. This kind of simple approach can be easily generalized to other types of geochemical parameters such as isotopic elements.

Seismic profiles have long been used to infer the mineralogy of the mantle (*Birch*, 1952). The competing petrological models for the upper mantle and transition zone are pyrolite (*Ringwood*, 1975) and piclogite (*Anderson and Bass*, 1984, 1986). So far, the isotropic seismic velocities can be explained down to 400km by a pyrolite model, but in the transition zone, indifferently by pyrolite or piclogite. *Montagner and Anderson* (1989a) investigated the correlations between anisotropic parameters for realistic mineralogical and petrological models of the upper mantle. They show that the anisotropic parameters involved in a radiallly anisotropic medium A, C, F, L, N are strongly correlated but that the 8 other anisotropic parameters $B_c, B_s, G_c, G_s, H_c, H_s, E_c, E_s$ involved in azimuthal anisotropy are less correlated. A complete exploitation of 3D anisotropic tomographic models has not yet been done. This kind of approach might provide in the next future some important constraints on mineralogy in the deep mantle.

The strain field near the surface is probably different from the deep one and could also be related to the strain field prevailing during the setting of materials. This shallow anisotropy could be very useful for understanding the strain field responsible for surficial tectonics. For example, seismic anisotropy could be used for explaining geological observations, such as mountain range building or more generally continental deformation. Such an application is attempted by *Vinnik et al.* (1989a,b; 1992), *Silver and Chan* (1988, 1991) and *Silver* (1996) by using anisotropy derived from SKS splitting. The poor lateral resolution of large scale anisotropic tomography can be considered as a strong limitation in continental areas. This technique can only be efficiently applied to areas where large scale strain and stress fields are implied. By applying this technique to Central Asia, *Griot et al.* (1998a,b) were able to discriminate between 2 extreme models of deformations, the heterogeneous model of *Avouac and Tapponnier* (1993) and the homogeneous model of *England and Houseman* (1986). They show that the heterogeneous model is in better agreement with observations in the first uppermost 200km of depth, whereas the homogeneous model better fits the deep anisotropy below 200km. This result provides a rough estimate on the thickness of the continental lithosphere.

All these examples show that that anisotropic tomography is still largely unexploited by the community of Earth scientists and will constitut an invaluable source of information and inspiration.

5 Conclusions

We have presented in this paper some basic first-order asymptotic theories which make it possible to derive anisotropic tomographic models. It was also shown that the phase information can be more easily interpreted in terms of structural parameters than the amplitude information.

That is the reason why seismologists primarily worked on the phase of seismograms rather than on its amplitude. This fundamental distinction between phase and amplitude results from the Fermat's principle (or Rayleigh's principle) which states that the propagation time (directly related to phase) is stationary to second order with respect to path perturbations, contrarily to the amplitude of waves. By applying the anisotropic technique to seismic data which makes use of the full potential of the 3 component seismograms, seismologists are able to image not only temperature anomalies but also to map the flow of matter in the Earth mantle.
The next steps will consist in taking a simultaneous account of phase and amplitude of seismic waves. By using new theoretical developments (*Clévdé and Lognonné*, 1997), it will be possible to calculate synthetic seismograms in complex *a priori* laterally heterogeneous media and to make a direct comparison with seismic waveform in time domain. And it will be possible to correctly assess the effect of scattering on seismograms. Notwithstanding these theoretical improvements, it should be desirable to increase the lateral resolution of tomographic models, in order to obtain images in a broad spatial scale range. This will be done, firstly, by installing broadband networks at smaller scale (wavelengths smaller than 1000km), and secondly by implementing an ocean seismic network, which will provide a better coverage of the whole Earth by seismic waves.

Ackowledgments CNRS UMR 7580 - Institut Universitaire de France - Institut d Physique du Globe.
This is I.P.G.P. contribution # .

References

REFERENCES

Agnew, D., J. Berger, R. Buland, W. Farrell and F. Gilbert, International deployment of accelerometers: A network of very long period seismology, *EOS, Trans. Am. Geophys. Un.*, **57**, 180-188, 1976.

Aki, K., and K. Kaminuma, Phase velocity of Love waves in Japan (part 1): Love waves from the Aleutian shock of March 1957, *Bull. Earthquake Res. Inst.*, **41**, 243–259, 1963.

Aki, K., and P. G. Richards, *Quantitative Seismology: Theory and Methods*, W. H. Freeman, San Fransisco, 1980.

Anderson, D. L., Elastic wave propagation in layered anisotropic media, *J. Geophys. Res.*, **66**, 2953-2963, 1961.

Anderson, D. L., *Theory of the Earth*, Blackwell scientific publications, Oxford, 1989.

Anderson, D. L., and J. D. Bass, Mineralogy and composition of the upper mantle, *Geophys. Res. Lett.*, **11**, 637-640, 1984.

Anderson, D. L., and J. D. Bass, Transition region of the Earth's upper mantle, *Nature*, **320**, 321-328, 1986.

Anderson, D. L., and A. M. Dziewonski, Upper mantle anisotropy: Evidence from fre oscillations, *Geophys. J. R. Astron. Soc.*, **69**, 383-404, 1982.

Ando, M., ScS polarization anisotropy around the Pacific Ocean, *J. Phys. Earth*, **32**, 179–196, 1984.

Ando, M., Y. Ishikawa and F. Yamazaki, Shear wave polarization anisotropy in the upper mantle beneath Honshu, Japan, *J. Geophys.Res.*, **88**, 5850–5864, 1983.

Ansel, V., and H.C Nataf, Anisotropy beneath 9 stations of the Geoscope broadband network as deduced from shear wave splitting, *Geophys. Res. Lett.*, **16**, 409–412, 1989.

Avouac, J.-P., and P. Tapponnier, Kinematic model of active deformation in central Asia, *Geophys. Res. Lett.*, **20**, 895-898, 1993.

Babuska, V., and M. Cara, Seismic Anisotropy in the Earth, Kluwer Acdemic Press, Dordrecht, The Netherlands, 1991.

Babuska, V., J.-P. Montagner, J. Plomerova, and N. Girardin, Age-dependent large-scale fabric of the mantle lithosphere as derived from surface-wave velocity anisotropy, *Pure Appl. Geophys.*, **151**, 257-280, 1998.

Backus, G. E., and F. Gilbert, Numerical applications of a formalism for geophysical inverse problems, *Geophys. J. R. Astron. Soc.*, **13**, 247-276, 1967.

Backus, G. E., and J. F. Gilbert, The resolving power of gross earth data, *Geophys. J. R. Astron. Soc.*, **16**, 169-205, 1968.

Backus, G. E., and F. Gilbert, Uniqueness in the inversion of inaccurate gross earth data, *Philos. Trans. R. Soc. London, Ser. A*, **266**, 123-192, 1970.

Barruol, G., and D. Mainprice, A quantitative evaluation of the contribution of crustal rocks to the shear-wave splitting of teleseismic SKS waves, *Phys. Earth Planet. Int.*, **78**, 281-300, 1993.

Barruol, G., P.G. Silver, and A. Vauchez, Shear wave splitting in the Eastern U.S.: deep structure of a complex continental plate, *J. Geophys. Res.*, **102**, 8329- 8348, 1997.

Bass, J. and D.L. Anderson, Composition of the upper mantle: Geophysical tests of two petrological models, *Geophys. Res. Lett.*, **11**, 237-240, 1984.

Bowman, J.R., and M. Ando, Shear-wave splitting in the upper mantle wedge above the Tonga subduction zone, *Geophys. J.R. Astron. Soc.*, **88**, 25–41, 1987.

Cacho, S., Etude et Réalisation d'un sismomètre très large bande, 3 axes, qualifié spatial, Thèse de l'Université Paris VII, 1996.

Cara, M., Regional variations of Rayleigh-mode velocities: a spatial filtering method, *Geophys. J; R. Astr. Soc.*, **57**, 649-670, 1978.

Cara, M., and J. J. Leveque, Anisotropy of the asthenosphere: The higher mode data of the Pacific revisited, *Geophys. Res. Lett.*, **15**, 205-208, 1988.

Cazenave, A., A. Souriau, and K. Dominh, Global coupling of Earth surface topography with hotspots geoid and mantle heterogeneities, *Nature*, **340**, 54–57, 1989.

Christensen, N.I., and S. Lundquist, Pyroxene orientation within the upper mantle, *Bull. Geol. Soc. Am.*, **93**, 279-288, 1982.

Clévédé, E., and P. Lognonné, Fréchet derivatives of coupled seismograms with to an anelastic rotating Earth, *Geophys. J. Int.*, **124**, 456-482 , 1996.

Crampin, S., An introduction to wave propagation in anisotropic media, *Geophys. J. R. Astron. Soc.*, **76**, 17–28, 1984.

Debayle, E., and J.-J. Lévêque, Upper mantle heterogeneities in the Indian Ocean froml waveform inversion, *Geophys. Res. Lett.*, **24**, 245-248, 1997.

Dost, B., Upper mantle structure under western Europe from fundamental and higher mode surface waves using the NARS array, *Geophys. J; R. Astron. Soc.*, **100**, 131-151, 1990.

Dziewonski, A. M., Mapping the lower mantle: Determination of lateral heterogeneity in P velocity up to degree and order 6, *J. Geophys. Res.*, **89**, 5929-5952, 1984.

Dziewonski, A. M., and D. L. Anderson, Preliminary Reference Earth Model, *Phys. Earth Planet. Int.*, **25**, 297–356, 1981.

Dziewonski, A. M., and J. H. Woodhouse, Global images of the Earth's interior, *Science*, **236**, 37-48, 1987.

England, P., and G. Houseman, Finite strain calculations of continental deformation, 2. comparison with the India-Asia collision zone, *J. Geophys. Res.*, **91**, 3664–3676, 1986.

Fisher, R.A., Dispersion on a sphere, *Proc. Roy. Soc.*, **A 217**, 295, 1953

Forsyth, D. W., The early structural evolution and anisotropy of the oceanic upper mantle, *Geophys. J. R. Astron. Soc.*, **43**, 103-162, 1975.

Gaherty, J.B., and T.H. Jordan, Lehmann discontinuity as the base of the anisotropic layer beneath continents, *Science, 268*, 1468- 1471, 1995.

Griot, D.-A., J.-P. Montagner, and P. Tapponnier, Surface wave phase velocity and azimuthal anisotropy in Central Asia, *J. Geophys. Res.*, **103** , 21215–21232, 1998a.

Griot, D.-A., J.-P. Montagner, and P. Tapponnier, Heterogeneous versus homogeneous strain in Central Asia, *Geophys. Res. Lett.*, **25**, 1447-1450, 1998b.

Hadiouche, O., N. Jobert and J.P. Montagner, Anisotropy of the African continent inferred from surface waves, *Phys. Earth Planet. Int., 58*, 61–81, 1989.

Hager, B.H., R.W. Clayton, M.A. Richards, R.P. Comer, and A.M. Dziewonski, Lower mantle heterogeneity, dynamic topography and the geoid, *Nature*, **313**, 541-545, 1985.

Hess, H., Seismic anisotropy of the uppermost mantle under the oceans, *Nature*, **203**, 629–631, 1964.

Ho-Liu, P., J.-P. Montagner, and H. Kanamori, Comparison of iterative back-projection inversion and generalized inversion without blocks: Case studies in Attenuation tomography, *Geophys. J.*, **97**, 19-29, 1989.

Knopoff, L., Observation and inversion of surface wave inversion, *Tectonophys.*, **13**, 497-519, 1972.

Larson,E.W., J. Tromp, and G. Ekstrom, Effects of slight anisotropy on surface waves, *Geophys. J. Int.*, **132**, 654-666, 1998.

Laske, G., and G. Masters, Surface-wave polarization data and global anisotropic structure, *Geophys. J. Int.*, **132**, 508-520, 1998.

Lerner-Lam, A.L., and T.H. Jordan, Earth structure from fundamental and higher-mode waveform analysis, *Geophys. J.R. astr. Soc.*, **75**, 759-797, 1983.

Lévêque, J.J., and M. Cara, Inversion of multimode surface wave data: evidence for sub–lithospheric anisotropy, *Geophys. J.R. astr. Soc.*, **83**, 753–773, 1985.

Lévêque, J.J., M. Cara, and D. Rouland, Waveform inversion of surface-wave data: a new tool for systematic investigation of upper mantle structures, *Geophys. J. Int.*, **104**, 565-581, 1991.

Levshin, A., and L. Ratnikova, Apparent anisotropy in inhomogeneous media, *Geophys. J.R. astr. Soc.*, **76**, 65-69, 1984.

Lognonné, P., J. Gagnepain-Beyneix, W.B. Banerdt, S. Cacho, and, J.-F. Karczewski, An ultra-broadband seismometer in InterMarsnet, *Planet. Space Sci.*, **44**, 1237-1249, 1996.

Masters, G., T.H. Jordan, P.G. Silver, and F. Gilbert, Aspherical Earth structure from fundamental spheroidal-mode data, *Nature*, **298**, 609-613, 1982.

Minster, J. B., and T. H. Jordan, Present-day plate motions, *J. Geophys. Res.*, **83**, 5331-5354, 1978.

Nolet, G., and B.J. Kennett, Normal-mode representation of multiple ray reflections in a spherical Earth, *Geophys. J. R. Astr. Soc.*, **53**, 219-226, 1978.

Okal, E., and B.-G. Jo, stacking investigation of higher-order mantle Rayleigh waves, *Geophys. Res. Lett.*, **12**, 421-424, 1985.

Peselnick, L., A. Nicolas, and P.R. Stevenson, Velocity anisotropy in a mantle peridotite from Ivrea zone: Application to uper mantle anisotropy, *J. Geophys. Res.*, **79**, 1175-1182, 1974.

Peselnick, L., and A. Nicolas, Seismic anisotropy in an ophiolite peridotite. Application to oceanic upper mantle, *J. Geophys. Res.*, **83**, 1227-1235, 1978.

Peterson, J., Observation and modeling of background seismic noise, *I.S. Geol. Surv. Open-file report 93-222*, Albuberque, 1993.

Peterson, J., H. M. Butler, L. G. Holcomb and C. R. Hutt, The Seismic Research Observatory, *Bull. Seism. Soc. Am.*, **66**, 2049-2068, 1977.

Ribe, N.M., Seismic anisotropy and mantle flow, *J. Geophys. Res.*, **94**, 4213-4223, 1989.

Ricard, Y., H.-C. Nataf, and J.-P. Montagner, The 3S-Mac model: confrontation with seismic data, *J. Geophys. Res.*, **101**, 8457-8472, 1996.

Richards, M. A., and B. H. Hager, The Earth's geoid and the large scale structure of mantle convection, in: *The Physics of the Planets*, S. J. Runcorn (Ed.), 247-271, 1988.

Ringwood, A.E., Composition and petrology of the Earth's mantle, McGraw–Hill, New–York, 618pp, 1975.

Romanowicz, B., The upper mantle degree two: Constraints and inferences from global mantle wave attenuation measurements, *J. Geophys. Res.*, **95**, 11,051- 11,071, 1990.

Romanowicz, B., M. Cara, J. F. Fels, and D. Rouland, GEOSCOPE: a French initiative in long period, three component, global seismic networks, *EOS, Trans. Am. Geophys. Un.*, **65**, 753-754, 1984.

Roult, G., B. Romanowicz, and J.-P. Montagner, 3D upper mantle shear velocity and attenuation from fundamental mode free oscillation data, *Geophys. J. Int.*, **101**, 61-80, 1990.

Silveira, G., E. Stutzmann, J.-P. Montagner and L. Mendes-Victor, Anisotropic tomography of the Atlantic Ocean from Rayleigh surface waves, *Phys. Earth Planet. Int.*, **106**, 259-275, 1998.

Silver, P.G., Seismic anisotropy beneath the continents: Probing the depths of geology, *Ann. Rev. Earth Planet. Sci.*, **24**, 385-432, 1996.

Silver, P.G., and W.W. Chan, Implications for continental structure and evolution from seismic anisotropy, *Nature*, **335**, 34–39, 1988.

Silver, P.G., and W.W. Chan, Shear wave splitting and subcontinental mantle deformation, *J. Geophys. Res.*, **96**, 16,429– 16,454, 1991.

Smith, S. W., IRIS; a program for the next decade, *EOS, Trans. Am. Geophys. Un.*, **67**, 213-219, 1986.

Smith, M. L., and F. A. Dahlen, The azimuthal dependence of Love and Rayleigh wave propagation in a slightly anisotropic medium, *J. Geophys. Res.*, **78**, 3321-3333, 1973.

Smith, M. L., and F. A. Dahlen, Correction to 'The azimuthal dependence of Love and Rayleigh wave propagation in a slightly anisotropic medium', *J. Geophys. Res.*, **80**, 1923, 1975.

Snieder, R., Large-scale waveform inversions of surface waves for lateral heterogeneity, 1. Theory and numerical examples, *J. Geophys. Res.*, **93**, 12,055-12,066, 1988a.

Snieder, R., Large-scale waveform inversions of surface waves for lateral heterogeneity, 2. Application to surface waves in Europe and the Mediterranean, *J. Geophys. Res.*, **93**, 12,067-12,080, 1988b.

Snieder, R., and B. Romanowicz, A new formalism for the effect of lateral heterogeneity on normal modes and surface waves, I: Isotropic perturbations, perturbations of interfaces and gravitational perturbations, *Geophys. J. R. Astron. Soc.*, **92**, 207-222, 1988.

Stutzmann, E., and J.P. Montagner,Tomography of the transition zone from the inversion of higher-mode surface waves, *Phys. Earth Planet. Int.*, **86**, 99-116, 1994.

Su, W.J., and A.M. Dziewonski, Predominance of long-wavelength heterogeneity in the mantle, *Nature*, **352**, 121-126, 1991.

Su, W.J., and A.M. Dziewonski, On the scale of mantle heterogeneity, *Phys. Earth Planet. Inter.*, **74**, 29-54, 1992.

Su, W.J., R.L. Woodward, and A.M. Dziewonski, *Nature*, **360**, 149-152, 1992.

Su, L., J. Park, and Y. Yu, Born seismograms using coupled free oscillations: the effect of strong coupling and anisotropy, *Geophys. J. Int.*, **115**, 849-862, 1993.

Suetsugu, D., and I. Nakanishi, Regional and azimuthal dependence of phase velocities of mantle Rayleigh waves in the Pacific Ocean, *Phys. Earth Planet. Int.*, **47**, 230–245, 1987.

Suyehiro, K., T. Kanazawa, N. Hirata, M. Shinohara, and H. Kinoshita, Broadband downhole digital seismometer experiment at site 794: a technical paper, Proc. ODP, Sc. Results, 127-128, 1992.

Takeuchi, H., and M. Saito, Seismic surface waves, *Methods Comput. Phys.*, **11**, 217-295, 1972.

Tanimoto, T., A simple derivation of the formula to calculate synthetic long period seismograms in a heterogeneous earth by normal mode summation, *Geophys. J. R. Astron. Soc.*, **77**, 275-278, 1984a.

Tanimoto, T., Waveform inversion of mantle Love waves: The Born seismogram approach, *Geophys. J. R. Astron. Soc.*, **78**, 641-660, 1984b.

Tanimoto, T., The Backus-Gilbert approach to the three-dimensional structure in the upper mantle, 1. Lateral variation of surface wave phase velocity with its error and resolution, *Geophys. J. R. Astron. Soc.*, **82**, 105-123, 1985.

Tanimoto, T., Free oscillations in a slightly anisotropic Earth, *Geophys. J. R. Astron. Soc.*, **87**, 493-517, 1986.

Tanimoto, T., Long-wavelength S-wave velocity structure throughout the mantle, *Geophys. J. Int.*, **100**, 327-336, 1990.

Tanimoto, T., and D. L. Anderson, Lateral heterogeneity and azimuthal anisotropy of the upper mantle: Love and Rayleigh waves 100–250s, *J. Geophys. Res.*, **90**, 1842-1858, 1985.

Tarantola, A., and B. Valette, Generalized non-linear inverse problems solved using the least squares criterion, *Rev. Geophys. Space Phys.*, **20**, 219-232, 1982.

Van der Hilst, R.D., and H. Karason, Compositional heterogeneity in the bottom 1000km of the Earth's mantle: Toward a hybrid convection model, *Science*, **283**, 1885-1888, 1999.

Van Heijst, H.J. and J. Woodhouse, Measuring surface-wave overtone phase velocities using a mode-branch stripping technique, *Geophys. J. Int.*, **131**, 209-230, 1997.

Vauchez, A., and A. Nicolas, Mountain building: strike-parallel motion and mantle anisotropy, *Tectonophys.*, **185**, 183-191, 1991.

Vinnik, L.P., G.L. Kosarev and L.I. Makeyeva, Anisotropiya litosfery po nablyudeniyam voln SKS and SKKS, *Doklady Akademii Nauk USSR*, **278**, 1335–1339, 1984.

Vinnik, L.P., R. Kind, G.L. Kosarev, and L.I. Makeyeva, Azimuthal Anisotropy in the lithosphere from observations of long–period S–waves, *Geophys. J. Int.*, **99**, 549–559, 1989a.

Vinnik, L.P., V. Farra, and B. Romanowicz, Azimuthal anisotropy in the earth from observations of SKS at GEOSCOPE and NARS broadband stations, *Bull. Seism. Soc. Am.*, **79**, 1542–1558, 1989b.

Vinnik, L., L.I. Makayeva, A. Milev, A.Y. Usenko, Global patterns of azimuthal anisotropy and deformations in the continental mantle, *Geophys. J. Int., 111*, 433-447, 1992.

Vinnik, L., B. Romanowicz, Y. Le Stunff, and L. Makayeva, Seismic anisotropy in D"-layer, *Geophys. Res. Lett.*, **22**, 1657- 1660, 1995.

Vinnik, L., an J.-P. Montagner, Shear wave splitting in the mantle from Ps phases, *Geophys. Res. Lett.*, **23**, 2449-2452, 1996.

Wielandt, E., and G. Streickeisen, The leaf-spring seismometer: design and performances, *Bull. Seism. Soc. Am.*, **72**, 2349-2367, 1982.

Woodhouse, J. H., and A. M. Dziewonski, Mapping the upper mantle: Three dimensional modelling of Earth structure by inversion of seismic waveforms, *J. Geophys. Res.*, **89**, 5953-5986, 1984.

Woodhouse, J. H., and Y. K. Wong, Amplitude, phase and path anomalies of mantle waves, *Geophys. J. R. Astron. Soc.*, **87**, 753-773, 1986.

Woodward, R. L., and G. Masters, Global uppper mantle structure from long-period differential travel-times, *J. Geophys. Res.*, **96**, 6351-6377, 1991a.

Woodward, R., and G. Masters, Lower-mantle structure from long period differential travel times, *Nature*, **352**, 231-233, 1991b.

Yu, Y., and J. Park, Anisotropy and coupled long-period surface waves, *Geophys. J. Int.*, **114** , 473-489, 1993.

Zhang, Y., and T. Tanimoto, High resolution global upper mantle structure; plate tectonics, *J. Geophys. Res.*, **98**, 9793-9823, 1993.